Analytical formulas for the performance scaling of quantum processors with a large number of defective gates

Y. S. Nam and R. Blümel

Department of Physics, Wesleyan University, Middletown, Connecticut 06459-0155, USA

(Received 11 March 2015; revised manuscript received 4 July 2015; published 1 October 2015)

Removing a single logical gate from a classical information processor renders this processor useless. This is not so for a quantum information processor. A large number of quantum gates may be removed without significantly affecting the processor's performance. In this paper, focusing on the quantum Fourier transform (QFT) and quantum adder, we show even more: Even if most of its gates are eliminated and the remaining gates are selected from a randomly generated set, the QFT, one of the most useful quantum processors, and the quantum adder, one of the most basic building blocks of a universal quantum computer, still operate with satisfactory success probability, comparable to that of a quantum computer constructed with perfect gates. We support these conclusions by first laying out a general analytical framework and then deriving analytical scaling relations, which are in excellent agreement with our numerical simulations. The demonstrated robustness of the QFT and quantum adder, to the point where randomly generated quantum gates take the place of the exact gates, is an important boon for the construction of quantum computers, since it shows that stringent gate error tolerances do not have to be met to obtain satisfactory performance of the corresponding quantum processors. Our analytical techniques are powerful enough to generate asymptotic scaling laws for any gate defect model of quantum information processors and we illustrate this point by explicitly computing asymptotic analytical scaling formulas for several other defect models as well.

DOI: 10.1103/PhysRevA.92.042301 PACS number(s): 03.67.Lx, 03.67.Ac

I. INTRODUCTION

More than two decades have passed since the discovery of Shor's algorithm [1], capable of factoring a semiprime faster than any known classical algorithm to date. Proving for the first time that a quantum computer is indeed practically useful and poses a threat to the widely employed Rivest-Shamir-Adleman cryptosystem [2], Shor's algorithm has attracted many scientists and engineers to the field of quantum computing, an interdisciplinary subject encompassing mathematics, computer science, physics, and chemistry with applications ranging from national security to search engines. To date, however, no universal quantum computer exists that is of practical interest. Even with novel breakthroughs such as fault-tolerant, error-correcting codes (see [3] and references therein), record-breaking experimental achievements in storing quantum information [4,5], and surface codes [6], the realization of practically useful quantum computers seems to lie in the distant future. Thus, in order to build a practical quantum computer, much work still needs to be done, in particular in the realm of robustness of quantum computers with respect to imprecise quantum hardware as will necessarily be found in any realistic implementation of a quantum processor.

It is no surprise, then, that there have been numerous investigations, both theoretical and experimental, studying the effects of imperfect hardware for a wide variety of quantum-computer architectures. In the field of Rydberg quantum processors, e.g., we find investigations of decoherence and fidelity of single- and two-qubit gates [7], a proposal of a new scheme for realizing a controlled-phase gate and quantifying its expected gate error level [8], studies of the effect of imperfections in the external hardware (e.g., control of field power or duration) on quantum-gate performance [9], and characterizations of the effect of errors accumulating over a sequence of single- and two-qubit gates [10]. Technological advances have resulted in reliable performance of Clifford gates in a spin-qubit system [11] with the reported error rate below the tolerable threshold required by surface codes [6]. Yet another advance has been reported by Zu *et al.* [12], where universal geometric rotation gates in a spin-qubit system have been experimentally realized. Experimental realization of the gates have also been reported in a superconducting system [13]. Recently, phase noise in a superconducting system has been characterized and investigated in detail in Ref. [14].

In this paper, further advancing the investigations of the effect of hardware errors on a quantum computer, we focus on the analytical analysis of the effects of gate errors in large-scale quantum processors. In particular, we develop analytical scaling laws that tell us how the processor's fidelity scales in the limit of a very large number of qubits. This is necessary since classical computers cannot simulate this quantum regime even in principle [15] and analytical scaling formulas, therefore, are the only way to assess the effects of imperfect gates in the practically relevant regime of a large number of qubits. In particular, analytical scaling formulas may give us an idea of the level of gate errors that may be tolerated for satisfactory quantum-computer performance in the large-scale limit. In addition, on the basis of these formulas, we may assess quantitatively whether a large-scale quantum processor reacts sensitively to gate errors or exhibits a more tolerant and robust response to gate errors.

We start with investigating the robustness of the quantum Fourier transform (QFT), one of the most important quantum information processors. Our choice is based on the universal applicability of the QFT in many useful quantum algorithms known to date (see [16] and references therein). For this reason, numerous works are available in the literature, investigating the robustness of the QFT, including approximation techniques [15,17–19], faulty gates [16,20–22], and structural stability

[23]. Further corroborating the robustness of the QFT is the random hierarchy approach [23], which we investigate in detail in this paper.

Yet another quantum processor we focus on in this paper is the quantum adder. As one of the most basic components of universal quantum computers, the quantum adder plays a central role in the construction of quantum arithmetic units [24]. Employing the QFT-based architecture [25], the respective quantum adder, mostly made of controlled rotation gates, will prove robust with respect to errors following a random hierarchy.

We shall demonstrate that in spite of deleting most of the controlled rotation gates from the QFT and quantum adder processors and replacing the remaining rotation gates with gates drawn from a small, randomly generated set, the quantum processors still display acceptable performance. We also derive explicit analytical scaling laws that support our prediction of robustness with respect to these drastic alterations of the QFT and quantum adder circuits.

Our paper is structured as follows. In Sec. II A, in the context of the QFT, we introduce the random hierarchy and present numerical results. Also introduced in this section is the concept of banding, a type of pruning technique that is necessary for practical quantum computing. Then, in Sec. II B we approach the same problem analytically and show that the resulting analytics and the numerical results found in Sec. II A are in excellent agreement. In Sec. III A we introduce the QFT-based quantum adder and its associated numerics in the context of gate errors including random hierarchy and banding. This is followed by Sec. III B, where we investigate the same problem analytically, whose results are once again in excellent agreement with the numerical results found in Sec. III A. Additionally, in Sec. III B we present analytical scaling laws of the performance of the quantum adder whose constituent quantum gates are subjected to perturbations whose statistical profiles follow normal or uniform distributions. Then, in Sec. IV we discuss our results. We summarize our paper in Sec. V.

II. ROBUSTNESS OF THE QFT

A. Numerics

An n-qubit QFT has exact rotation angles $\theta_j = \pi/2^j$, $j = 1,\ldots,n-1$, where j is the distance between control and target qubits (see Fig. 1 for a sample circuit of a five-qubit QFT). In order to investigate the robustness of the n-qubit QFT to a class

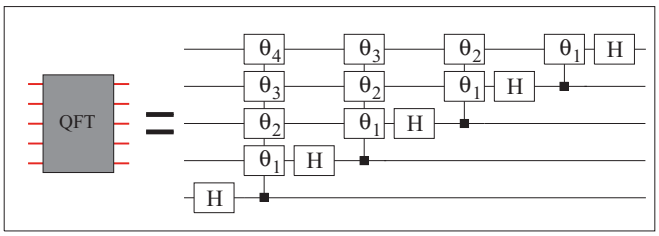

FIG. 1. (Color online) Logic circuit of a five-qubit QFT. Hadamard gates are denoted by H and phase rotation gates by θ_j, whose rotation angle is $\pi/2^j$ [26], where j is the qubit distance between control and target qubits.

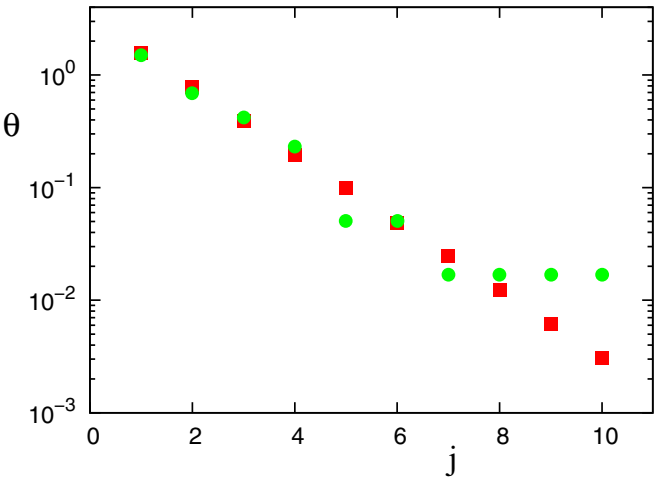

FIG. 2. (Color online) Exact rotation angles θ_j (red closed squares) compared with their corresponding approximations $\tilde{\theta}_j$ (green closed circles) as a function of qubit distance j for $j = 1,\ldots,10$. The approximations $\tilde{\theta}_j$ are the best matches for their corresponding θ_j, drawn from a set of $N = 20$ randomly generated rotation angles. The plateau in $\tilde{\theta}$ is a consequence of having small N, i.e., θ_j for $j \geqslant 7$ is approximated by the same approximate angle $\tilde{\theta}_j$. Although θ_j and $\tilde{\theta}_j$ appear to be close on a logarithmic scale, their percentage differences are large, exceeding 30% from $j = 7$ on. Nevertheless, a QFT equipped with these gates exhibits acceptable performance.

of drastic changes $\theta_j \to \tilde{\theta}_j$ of its rotation angles, we employ the following methodology. We produce a set S_N of $N \geqslant n-1$ random numbers, uniformly distributed in $(0,\pi)$. From S_N we draw those random numbers that are closest to the exact rotation angles θ_j (repetitions are permitted) and denote them by $\tilde{\theta}_j$. Since the new angles $\tilde{\theta}_j$ are drawn from the same random set S_N, but still constructed in such a way that they are ordered hierarchically in descending order, we call this implementation of the QFT a realization with a random hierarchy. Figure 2 illustrates the result of this procedure for $N = 20$. The red squares are the exact angles θ_j, while the green closed circles are the best matches $\tilde{\theta}_j$ for the exact angles θ_j, drawn from a set of $N = 20$ random numbers. Although seemingly close on the logarithmic scale of Fig. 2, the relative errors $r_j = |\tilde{\theta}_j - \theta_j|/\theta_j$ for this particular realization of random angles $\tilde{\theta}_j$ are large, ranging from 4% for $j = 1$ to 48% for $j = 5$, exceeding 100% from $j = 9$ on. These are large errors, deliberately introduced into the QFT, since our point is to show that even in the case of a random realization of rotation angles, the QFT still performs satisfactorily. Of course, in the limit $N \to \infty$, $\tilde{\theta}_j$ approaches θ_j. Our point, however, is that even if N is small, and consequently r_j may be large, the QFT still performs at an astonishingly high level.

We note that scaling noise models, such as perturbing the angles θ_j with noise whose level scales in the size of θ_j, for instance, have been studied in great detail for the QFT in Ref. [16]. In Sec. II B, where we discuss our analytical calculations, we will further establish how our work here connects to that in Ref. [16]. Our choice of the random hierarchy here is deliberate since the errors introduced by the random hierarchy are not adapted to the natural exponential behavior of the rotation angles in either the QFT or the quantum

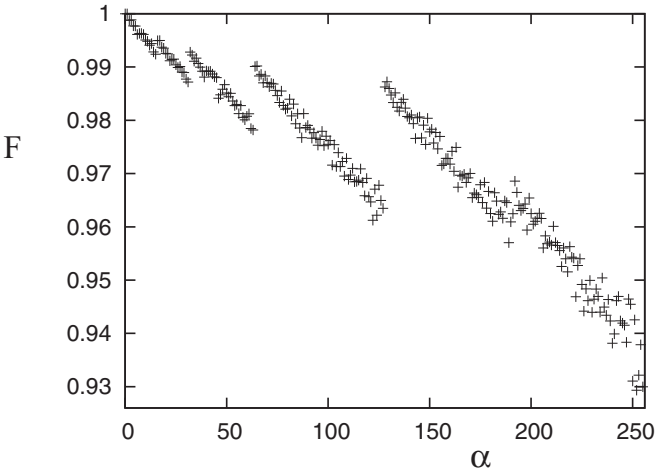

FIG. 3. Fidelity F of an eight-qubit QFT as a function of integer input state $|\alpha\rangle$. Each plot symbol is a result of averaging over 1000 realizations of the random set S_N, where $N = 30$ was used in this figure. As the bit spectra of α become filled with 1's, the fidelity F decreases. As expected, and proved in Appendix A, the case $\alpha = 2^8 - 1$ (rightmost point in the figure), where all bits of α are 1, returns the worst F.

adders. Thus this type of errors is a stringent test of the robustness of both the QFT and adder quantum processors.

We start with the statement that the QFT equipped with the random hierarchy performs at an astonishingly high level even when N is small. We denote by $\hat{\mathcal{Q}}$ the ideal QFT operation, equipped with θ_j gates, and by $\hat{\tilde{\mathcal{Q}}}$ the modified QFT operation, equipped with $\tilde{\theta}_j$ gates. As a test state for these two QFTs we choose $|\psi_{\text{in}}\rangle = |2^n - 1\rangle$ since this is the most unfavorable case for both QFTs. This is so because $|\psi_{\text{in}}\rangle$ ensures that all rotation gates in the QFT (see Fig. 1), together with their respective errors (in the case of $\hat{\tilde{\mathcal{Q}}}$), are always switched on. In contrast, choosing $|0\rangle$ as an input state would always result in perfect performance, even in the case of completely random rotation gates, since for this input state none of the rotation gates is triggered. To illustrate this point more clearly, we plot in Fig. 3 the fidelity of the QFT defined according to $F = \langle|\langle\psi_{\text{ideal}}|\psi_{\text{actual}}\rangle|^2\rangle$ as a function of α, where for any integer input state $|\psi_{\text{in}}\rangle = |\alpha\rangle$ the states $|\psi_{\text{ideal}}\rangle$ and $|\psi_{\text{actual}}\rangle$ are computed according to $|\psi_{\text{ideal}}\rangle = \hat{\mathcal{Q}}|\psi_{\text{in}}\rangle$ and $|\psi_{\text{actual}}\rangle = \hat{\tilde{\mathcal{Q}}}|\psi_{\text{in}}\rangle$ and the angular brackets in the definition of F indicate averaging over multiple realizations of the random set S_N. We observe that as more controlled-rotation gates turn on, i.e., the bit spectra of α get filled in with 1's, the fidelity F decreases. A detailed analytical proof demonstrating that $|2^n - 1\rangle$ is indeed the least-favorable input state is available in Appendix A.

Having chosen an appropriate test state, we now assess the performance of the modified QFT by computing the fidelity F, averaged over 100 realizations of the random set S_N, as a function of the number of qubits n. The result is shown in Fig. 4(a). As expected, the larger the number of randomly generated gates N, the better the quantum computer performs. In addition, as shown in Fig. 4(a), even with N as small as $N = 20$, a 17-qubit QFT still performs well above 30%. Figure 4(a) also shows that for fixed N the performance of the QFT decreases with increasing number of qubits n. This result is intuitively obvious since the more gates we need to approximate with only a finite number N of random gates at hand, the worse the performance of the quantum computer is expected to become.

We now band the QFT with bandwidth b, i.e., we prune those rotation gates from the QFT circuit whose ideal rotation angles are $\pi/2^j$, where $j > b$ [15,17–19]. The results for b=8 are shown in Fig. 4(b). Comparing with the corresponding cases of Fig. 4(a), we notice that the fidelity computed with $b = 8$ is significantly better than that with full bandwidth. This confirms the conjecture in Ref. [27] that banding, in the presence of imperfect hardware, boosts QFT performance by removing faulty rotation gates that do nothing useful but instead channel noise and errors into the still useful parts of the quantum processor. As a consequence, we expect that for given n and b there is a transition point N_c between the regimes of N in which banding increases ($N < N_c$) and decreases

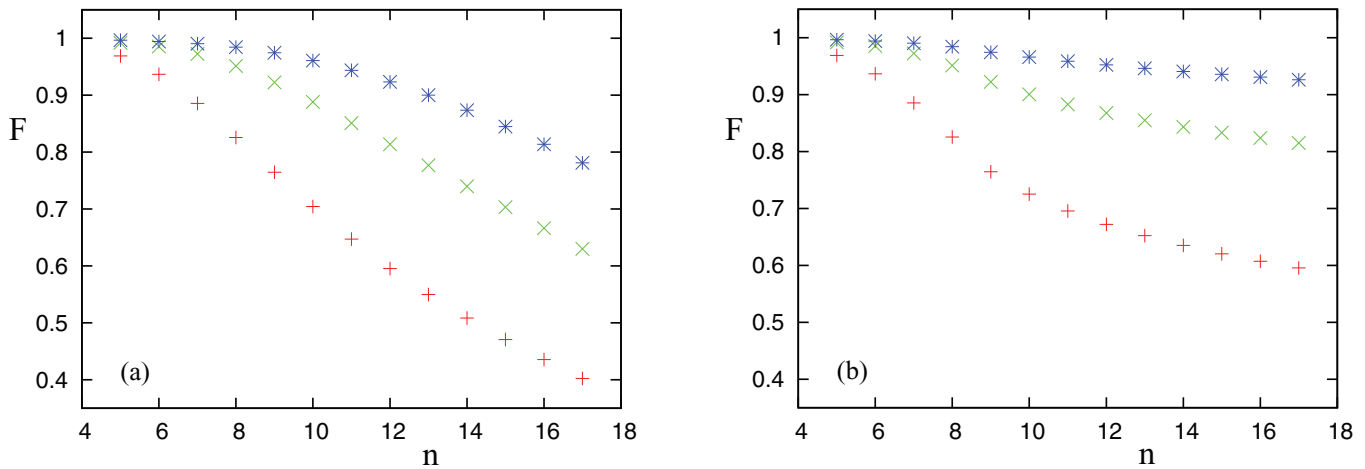

FIG. 4. (Color online) Fidelity F of the QFT equipped with the randomly hierarchical rotation gates $\tilde{\theta}_j$ as a function of the number of qubits n. Shown are the cases of $N = 20$ (red pluses), $N = 40$ (green crosses), and $N = 60$ (blue asterisks), each averaged over 100 ensembles of the respective S_N. (a) Full-bandwidth QFT and (b) banded QFT with bandwidth $b = 8$.

($N > N_c$) QFT performance. Thus, N_c is the critical N, where banding has no effect on the performance of the QFT. The latter regime is expected since for $N \to \infty$ the full-bandwidth QFT converges to $F = 1$, whereas the banded QFT converges to some constant F with $F < 1$. According to (46), derived in Sec. IV, $N_c = 470$ for the example ($n = 17$, $b = 8$) presented in Fig. 4. This explains that in this case banding substantially improves performance.

B. Analytics

While the numerical simulations help us see how the QFT performs when equipped with modified rotation gates, the practically interesting regime with thousands of qubits cannot ever be simulated on a classical computer. This regime can only be accessed via analytical calculations.

We start our analytical derivations by characterizing the statistics of the modified gates $\tilde{\theta}_j$. Writing $\tilde{\theta}_j = \theta_j + \epsilon_j$, we note that ϵ_j follows a bivariate exponential distribution function. This is so because the probability of finding the closest random number $\tilde{\theta}_j$ to θ_j within a distance d for N given random numbers, distributed uniformly between 0 and π, scales like $[(\pi - 2d)/\pi]^N$, which, for $d \sim \pi/N$ and large N, may be written as $\exp(-2Nd/\pi)$. According to this point of view, the random hierarchy QFT studied here is no different from the absolute typed error case studied in Ref. [16], except for the fact that the statistical distribution of the perturbing term ϵ_j is now bivariate exponential, rather than uniform, as was the case in Ref. [16].

While the performance criterion used in Ref. [16] (nearest-peak criterion) is not identical with the criterion used in this paper (fidelity), we note that, in the limit in which the perturbation is small, the two criteria are interchangeable. This is so because the fidelity $F = \langle|\langle\psi_{\text{ideal}}|\psi_{\text{actual}}\rangle|^2\rangle$ can be rewritten as $\langle|\sum_\beta \Phi^*(\alpha,\beta)\tilde{\Phi}(\alpha,\beta)|^2\rangle$, where

$$|\psi_{\text{ideal}}\rangle = \hat{\mathcal{Q}}|\psi_{\text{in}}\rangle = \sum_\beta \Phi(\alpha,\beta)|\beta\rangle, \tag{1}$$

with $|\psi_{\text{in}}\rangle = |\alpha\rangle$ for α an integer, and a similar expression for the modified QFT with $\hat{\tilde{\mathcal{Q}}}$ and $\tilde{\Phi}(\alpha,\beta)$. Assuming that the perturbation phase $\Delta\Phi^{(\text{def})}$, defined according to $\tilde{\Phi}(\alpha,\beta) = \Phi(\alpha,\beta)\Delta\Phi^{(\text{def})}(\alpha,\beta)$, fluctuates rapidly, we arrive at the analytical fidelity expression

$$F \approx \langle|\langle\Delta\Phi^{(\text{def})}(\alpha,\beta)\rangle_\beta|^2\rangle, \tag{2}$$

where $\langle\cdots\rangle_\beta$ denotes averaging over β, which is identical to Eq. (33) of Ref. [16] up to summation. Summation, however, is irrelevant, as we further assume for the following statistical analysis that the bits in both the input α and the output β are random sequences of 0's and 1's.

Closely following the steps of the analytical analysis developed in Ref. [16] and taking care to replace the uniform distributions assumed in Ref. [16] with the bivariate exponential probability distribution of the difference angles ϵ_j, we obtain the analytical fidelity function of the randomly hierarchical, full-bandwidth QFT to be

$$F \approx \exp\left[\frac{-n(n-1)}{8(2N/\pi)^2}\right]. \tag{3}$$

In order to demonstrate the quality of our analytical results, we plot in Fig. 5(a) the complement $1 - F$ of the fidelity F of the full-bandwidth QFT as a function of N for various n values, obtained from numerical simulations (plot symbols), together with the analytical results (3) (solid lines). The analytical results match the numerical results to an excellent degree. As expected, the fit is better in the large-N regime (small ϵ_j), demonstrating that the analytical results capture the scaling in both n and N correctly.

At this point, we introduce banding in our analytical analysis. Once again we start with the fidelity definition, only this time we have $F_b = \langle|\langle\psi_{\text{ideal}}|\psi_{\text{banded}}\rangle\langle\psi_{\text{banded}}|\psi_{\text{actual}}\rangle|^2\rangle$ with

$$|\psi_{\text{banded}}\rangle = \hat{\mathcal{Q}}_b|\psi_{\text{in}} = \alpha\rangle = \sum_\beta \Phi_b(\alpha,\beta)|\beta\rangle, \tag{4}$$

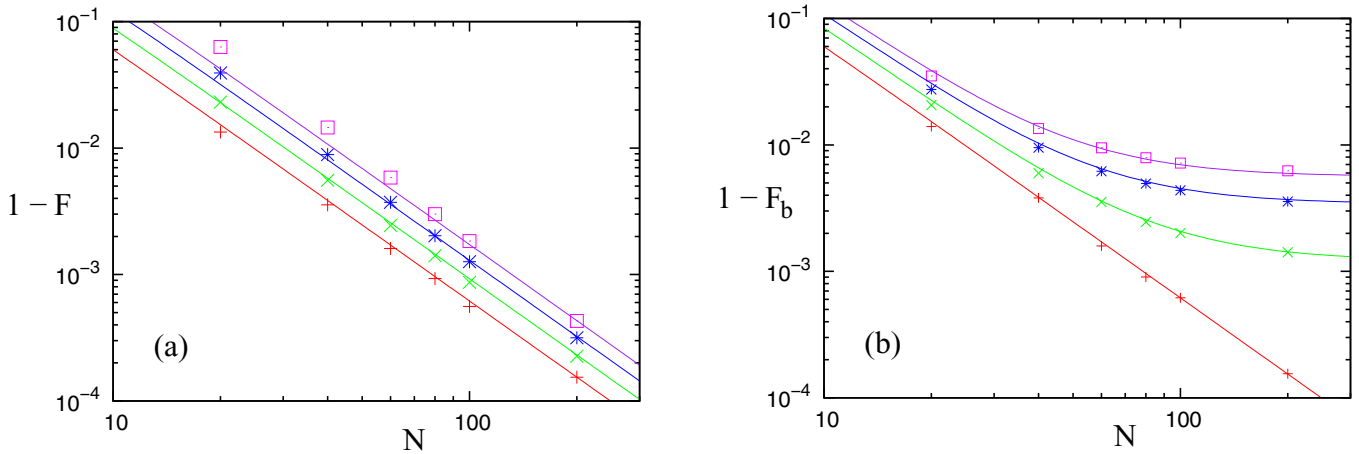

FIG. 5. (Color online) Complement $1 - F$ of the fidelity F of the QFT equipped with the randomly hierarchical rotation gates $\tilde{\theta}_j$ as a function of the number of random gates N. In order to match the random bit spectrum assumption used in the analytical calculations, all numerical simulation data are averaged over all possible integer input states $|\alpha\rangle$, where $\alpha = 0, \ldots, 2^n - 1$, for an n-qubit QFT, in addition to the averaging over 100 realizations of N random gates. (a) Full-bandwidth QFT and (b) banded QFT with bandwidth $b = 4$. Shown are the cases with $n = 5$, 6, 7, and 8, corresponding to pluses (red), crosses (green), asterisks (blue), and squares (purple), respectively.

where $\hat{\mathcal{Q}}_b$ and Φ_b denote the banded QFT operator and the associated phase with bandwidth b, respectively. Assuming (i) a statistical independence between $\langle\psi_{\text{ideal}}|\psi_{\text{banded}}\rangle$ and $\langle\psi_{\text{banded}}|\psi_{\text{actual}}\rangle$ and (ii) a rapidly fluctuating, random hierarchy perturbation phase $\Delta\Phi_b^{(\text{def})}$, defined according to $\tilde{\Phi}_b(\alpha,\beta) = \Phi_b(\alpha,\beta)\Delta\Phi_b^{(\text{def})}(\alpha,\beta)$, where $\tilde{\Phi}_b(\alpha,\beta)$ denotes the modified banded QFT phase, we arrive at the analytical banded QFT fidelity expression

$$F_b \approx \left|\sum_\beta \Phi^*(\alpha,\beta)\Phi(\alpha,\beta)e^{i\phi_b(\alpha,\beta)}\right|^2 \times \left\langle\left|\left\langle\Phi_b^*(\alpha,\beta)\Phi_b(\alpha,\beta)\Delta\Phi_b^{(\text{def})}(\alpha,\beta)\right\rangle_\beta\right|^2\right\rangle, \quad (5)$$

where we used $\Phi_b = \Phi e^{i\phi_b}$ and ϕ_b denotes the phase-angle offset of Φ_b from Φ, arising from banding with bandwidth b. Together with $|\sum_\beta \Phi^*\Phi e^{i\phi_b}|^2 \approx |\langle e^{i\phi_b}\rangle_\beta|^2$, assuming a rapidly fluctuating ϕ_b, and using the results derived in Refs. [15,16], we obtain

$$F_b \approx \exp\left[-\frac{\pi^2 2^{-2b}(n-b-1)+\delta}{12}\right] \times \exp\left[-\frac{nb-b(b+1)/2}{4(2N/\pi)^2}\right], \quad (6)$$

where $\delta = c(n-b)$ (c is a constant) is a small offset, which is due to residual correlations not included in our statistical analysis. Its linear dependence on n is expected since δ represents the residual inaccuracy in finding the variance of the accumulated phase angles, which scales like $\sim n$. The constant c is determined by fitting to simulation data. For $b = 4$, e.g., the best fit is obtained for $\delta = -0.012(n-b)$ for $n > b+1$. Figure 5(b) shows that for this choice of δ, the analytical scaling formula F_b in Eq. (6) matches the numerical simulation results to an excellent degree.

III. ROBUSTNESS OF THE QUANTUM ADDER

A. Numerics

So far, we investigated the robustness of the QFT in detail, both analytically and numerically. In this section, we extend our analysis to a quantum adder, the fundamental component of quantum arithmetics, which is universally applicable to any serious quantum computation. In particular, we investigate a quantum Fourier adder [25], shown in Fig. 6, which also serves as a test-bed application of the QFT processor that has been analyzed in detail in Secs. II A and II B. Hereafter, we make the following distinction: We refer to the quantum circuit that performs a quantum addition as the quantum adder and the associated part of the circuit that performs an addition in Fourier space as the quantum Fourier adder (see Fig. 6).

To start with, we implement randomly hierarchical controlled rotation gates to our quantum adder. Since we now have an additional gate to approximate, i.e., a π gate denoted by θ_0, we extend the domain from which the random numbers are drawn from $(0,\pi)$ to $(0,2\pi)$. The results are shown in Fig. 7(a), where, consistent with the methodology presented in Sec. II A, we used the input state $|\psi_{\text{in}}\rangle = |2^n - 1\rangle$ and the addend $\nu = 2^n - 1$ for an n-qubit quantum adder. The analytical proof showing why this is statistically the least-favorable case scenario in terms of fidelity is provided in Appendix B. The

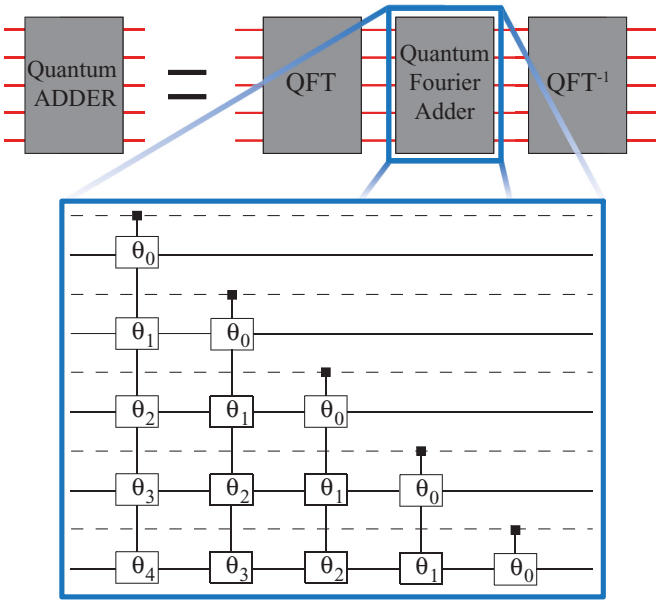

FIG. 6. (Color online) Logic circuit of a five-qubit quantum Fourier adder in the Fourier space (blue box). A complete quantum adder circuit requires both a QFT and an inverse QFT operation, performed before and after application of the quantum Fourier adder (see the top of the figure). Phase rotation gates are represented by the θ_j boxes; their respective rotation angles are $\pi/2^j$ [26], where j is the qubit distance between control and target qubits. The dashed lines represent the qubit lines of the addend ν of the adder. The solid lines represent the qubit lines of the computational qubits.

fidelity F, plotted against the number of qubits n, as expected, is larger when the number of randomly generated gates N increases. Furthermore, as shown in Fig. 7(a), even with N as small as 40, a 17-qubit quantum adder still performs at a level of about 20%. Figure 7(a) also shows that for fixed N the performance of the quantum adder decreases with increasing number of qubits n. This result, in analogy to the QFT, is intuitively obvious since the more gates we need to approximate with a finite number of random gates, the poorer the quality of the quantum processor becomes.

This time, we band the quantum adder with bandwidth b, deleting all rotation gates with their rotation angle less than $\pi/2^b$. Figure 7(b) shows the results for the case $b = 8$. Just as in the case of the QFT, we find that the banded quantum adder significantly outperforms the full-bandwidth quantum adder. For $N = 40$ and $n = 17$, for instance, i.e., the case we considered in connection with Fig. 7(a), the performance of the banded adder is above 30%, significantly better than the 20% performance of the adder without banding. This is consistent with the results reported in Sec. II A in connection with the QFT in the sense that erroneous gates with large j do more harm than good to the fidelity of a quantum processor by channeling noise into the system.

B. Analytics

We now approach the quantum adder fidelity problem analytically. We do this in two steps. First, we lay out a general analytical framework to arrive at the fidelity expression without specifying the types of errors. Only then, after obtaining the general fidelity expression, do we specify the types of

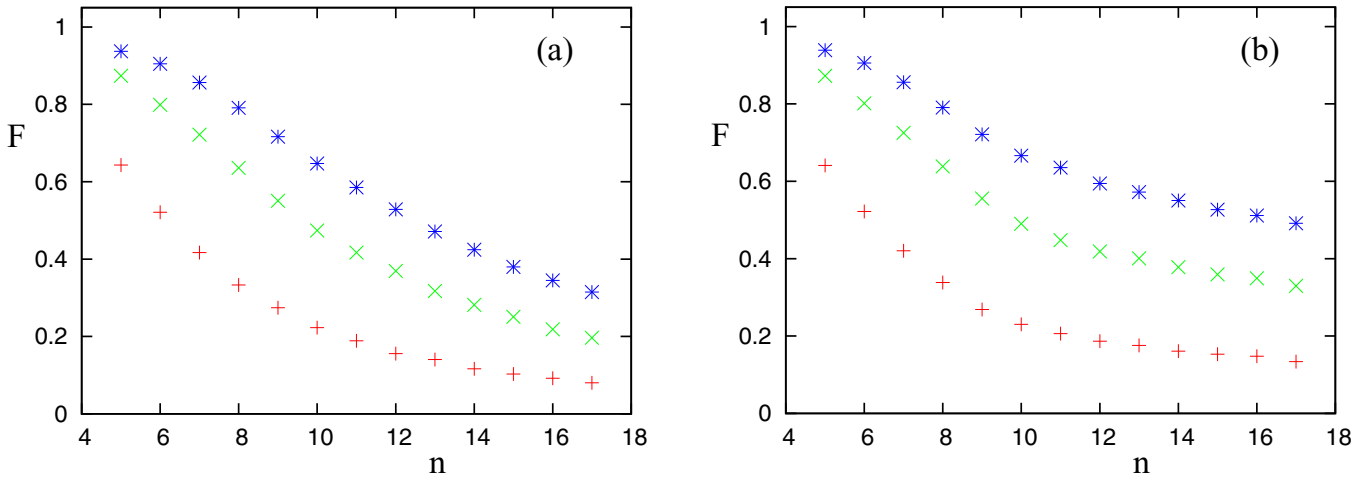

FIG. 7. (Color online) Fidelity F of the quantum adder equipped with the randomly hierarchical rotation gates $\tilde{\theta}_j$ as a function of the number of qubits n. Shown are the cases of $N = 20$ (red pluses), $N = 40$ (green crosses), and $N = 60$ (blue asterisks). Each plot symbol is a result of averaging over 10 000 ensembles of the random set S_N. (a) Full-bandwidth quantum adder and (b) banded quantum adder with bandwidth $b = 8$.

errors. This keeps our analytical results on the most general level, so that our analytical formulas are generally applicable to a wide range of error models. To demonstrate the general applicability of our analytical results to different kinds of error models, in this section, in addition to the random hierarchy, we also investigate Gaussian and uniformly distributed errors.

To start, we recall the definition of fidelity $F = \langle|\langle\psi_{\rm ideal}|\psi_{\rm actual}\rangle|^2\rangle$. Defining $\Phi^{(\rm QFA)}(\beta;\nu)$ as the phase associated with the quantum Fourier adder (see Fig. 6), where β is an integer input and ν is the addend of the adder, together with (1) and its inverse expression, we may write the quantum adder fidelity

$$F^{(\rm QA)} = \left\langle \left| \left(\sum_{\beta,\gamma} \langle\gamma|\Phi(\beta,\gamma)\Phi^{*(\rm QFA)}(\beta;\nu)\Phi^{*}(\alpha,\beta) \right) \left(\sum_{\beta',\gamma'} \tilde{\Phi}(\alpha,\beta')\tilde{\Phi}^{(\rm QFA)}(\beta';\nu)\tilde{\Phi}^{*}(\beta',\gamma')|\gamma'\rangle \right) \right|^2 \right\rangle, \tag{7}$$

where $\tilde{\Phi}$ and $\tilde{\Phi}^{(\rm QFA)}$ denote the phases of the defective QFT and quantum Fourier adders, respectively, and α is the input integer. Defining $\tilde{\Phi} = \Phi\Delta\Phi^{(\rm def)}$ and $\tilde{\Phi}^{(\rm QFA)} = \Phi^{(\rm QFA)}\Delta\Phi^{(\rm QFA)(\rm def)}$, together with $\langle\gamma|\gamma'\rangle = \delta_{\gamma,\gamma'}$, where δ is the Kronecker delta, (7) may now be written as

$$F^{(\rm QA)} = \left\langle \left| \left(\sum_{\beta} \Phi(\beta,\gamma)\Phi^{*(\rm QFA)}(\beta;\nu)\Phi^{*}(\alpha,\beta) \right) \times \left(\sum_{\beta'} \Phi(\alpha,\beta')\Phi^{(\rm QFA)}(\beta';\nu)\Phi^{*}(\beta',\gamma)\Delta\Phi^{(\rm def)}(\alpha,\beta')\Delta\Phi^{(\rm QFA)(\rm def)}(\beta';\nu)\Delta\Phi^{*(\rm def)}(\beta',\gamma) \right) \right|^2 \right\rangle. \tag{8}$$

Assuming that the defect phases fluctuate fast, we may approximate (8) as

$$F^{(\rm QA)} \approx \langle|\langle\Delta\Phi^{(\rm def)}(\alpha,\beta')\Delta\Phi^{(\rm QFA)(\rm def)}(\beta';\nu)\Delta\Phi^{*(\rm def)}[\beta',(\alpha+\nu) \bmod 2^n]\rangle_{\beta'}|^2\rangle, \tag{9}$$

where $\langle\cdots\rangle_{\beta'}$ denotes averaging over β' and n is the number of qubits. We note that the exact-adder parts in Eq. (8) evaluate to $\delta_{\gamma,(\alpha+\nu) \bmod 2^n}$, explaining the origin of the second argument $(\alpha+\nu) \bmod 2^n$ of the last term in Eq. (9). Further assuming a statistical independence between the three terms in Eq. (9), we obtain

$$F^{(\rm QA)} \approx \langle|\langle\Delta\Phi^{(\rm def)}(\alpha,\beta')\rangle_{\beta'}|^2\rangle\langle|\langle\Delta\Phi^{(\rm QFA)(\rm def)}(\beta';\nu)\rangle_{\beta'}|^2\rangle\langle|\langle\Delta\Phi^{*(\rm def)}[\beta',(\alpha+\nu) \bmod 2^n]\rangle_{\beta'}|^2\rangle. \tag{10}$$

Now we inspect each term in Eq. (10) individually. First, we recall that the defective phases arise from the defects included in phase-rotation gates. According to the analysis shown in Ref. [16], then, as long as the central limit theorem [28] on random phase-angle accumulation holds, without loss of generality, we may write

$$F^{(\rm QA)} \approx e^{-\sigma_n^2} e^{-[\sigma_n^{(\rm QFA)}]^2} e^{-\sigma_n^2}, \tag{11}$$

where σ_n and $\sigma_n^{(\rm QFA)}$ are the standard deviations of the defective phase angles accumulated from gate errors associated with an

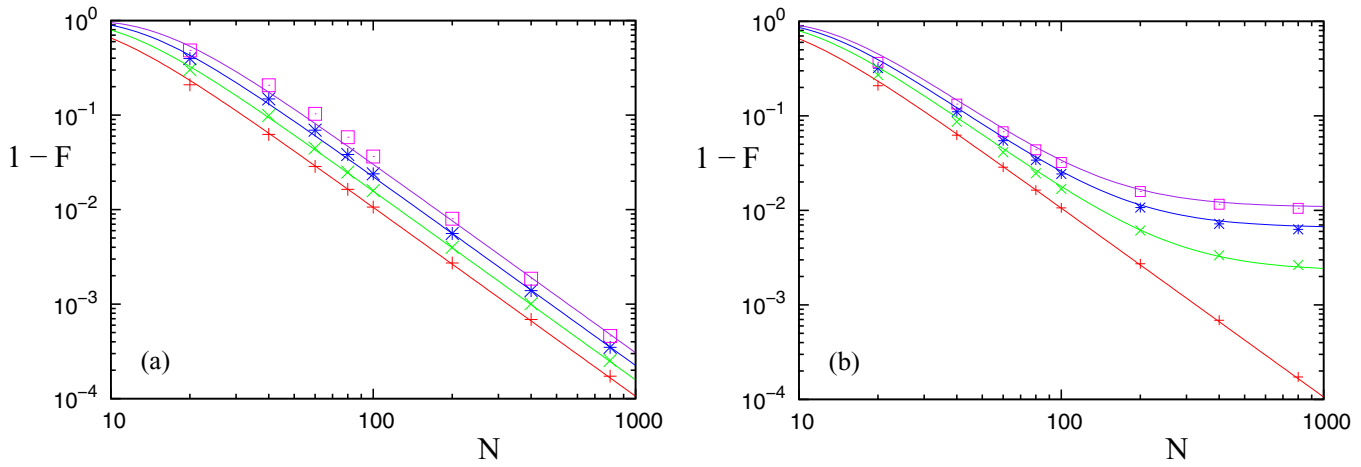

FIG. 8. (Color online) Complement $1-F$ of the fidelity F of the quantum adder equipped with the randomly hierarchical rotation gates $\tilde{\theta}_j$ as a function of the number of random gates N. In order to match the random bit spectrum assumption used in the analytical calculations, all numerical simulation data are averaged over all possible integer input states $|\alpha\rangle$, where $\alpha = 0, \ldots, 2^n - 1$ and all possible integer addends $\nu = 0, \ldots, 2^n - 1$. Shown are the results of averaging over 10 000 realizations of the random set S_N. (a) Full-bandwidth quantum adder and (b) banded quantum adder with bandwidth $b = 4$. The cases with $n = 5, 6, 7$, and 8 correspond to pluses (red), crosses (green), asterisks (blue), and squares (purple), respectively.

n-qubit QFT and an n-qubit quantum Fourier adder, respectively. Notice that there are two differences between the QFT and the quantum Fourier adder: (i) The quantum Fourier adder has no Hadamard gates, i.e., it purely consists of controlled phase-rotation gates, and (ii) compared to the QFT it has n additional π gates. With $[\sigma_n^{(\mathrm{QFA})}]^2 = 4(\sigma_n)^2 + n\langle\Delta\varphi_0^2\rangle/4$, where $\langle\Delta\varphi_0^2\rangle$ is the variance associated with the defect of a π phase-rotation gate, our general fidelity expression reads

$$F^{(\mathrm{QA})} \approx e^{-6\sigma_n^2 - n\langle\Delta\varphi_0^2\rangle/4}. \tag{12}$$

At this point we are ready to choose a specific type of error for the quantum adder fidelity expression. To this end, we insert the random hierarchy case into (12) and obtain, to leading order in n,

$$F_{\mathrm{RH}}^{(\mathrm{QA})} = \exp\left(-\frac{3n^2}{4(N/\pi)^2}\right). \tag{13}$$

We are not able to compute the next term in a systematic n expansion of the argument of the exponent in Eq. (13) analytically. However, we may take a cue from our work in Ref. [15]. Although focused on scaling relations of Shor's algorithm in the absence of noise, and therefore not directly related to our work here, [15] nevertheless suggests that the next-order correction term, which will dominate the other correction terms for $n \geqslant z$, should have the form

$$[s(n-u) - v]/(N/\pi)^2, \tag{14}$$

where s, u, v, and z are integer constants. Unable to determine these constants analytically, we determined them numerically. The best fit was found for $s = 3$, $u = 2$, $v = 1$, and $z = 5$. Therefore, adding the term $[3(n-2) - 1]/(N/\pi)^2$ for $n \geqslant 5$ to the exponent of (13), we obtain our final analytical formula, which is compared with numerical simulations in Fig. 8(a). We see that the analytical formula matches the numerical results to an excellent degree, i.e., the analytical formula correctly predicts the scaling of the quantum adder fidelity.

Closely following the steps outlined in Sec. II B, it can be shown that, in analogy to (10), the banded adder performs with fidelity

$$\begin{aligned} F_b^{(\mathrm{QA})} \approx{}& |\langle e^{i\phi_b(\alpha,\beta')}\rangle_{\beta'}|^2 \left|\left\langle e^{i\phi_b^{(\mathrm{QFA})}(\beta';\nu)}\right\rangle_{\beta'}\right|^2 \\ &\times |\langle e^{-i\phi_b(\beta',(\alpha+\nu) \bmod 2^n)}\rangle_{\beta'}|^2 \\ &\times \left\langle \left|\left\langle \Delta\Phi_b^{(\mathrm{def})}(\alpha,\beta')\right\rangle_{\beta'}\right|^2 \right\rangle \left\langle \left|\left\langle \Delta\Phi_b^{(\mathrm{QFA})(\mathrm{def})}(\beta';\nu)\right\rangle_{\beta'}\right|^2 \right\rangle \\ &\times \left\langle \left|\left\langle \Delta\Phi_b^{*(\mathrm{def})}[\beta',(\alpha+\nu) \bmod 2^n]\right\rangle_{\beta'}\right|^2 \right\rangle, \end{aligned} \tag{15}$$

where ϕ_b and $\phi_b^{(\mathrm{QFA})}$ denote, respectively, the phase-angle offsets associated with the QFT and the quantum Fourier adder due to banding and $\Delta\Phi_b^{(\mathrm{def})}$ and $\Delta\Phi_b^{(\mathrm{QFA})(\mathrm{def})}$ denote the respective defect phases. Using the results from Sec. II B, [15,16] and denoting the variance of the phase-angle defects of the banded QFT with bandwidth b as $\sigma_{n,b}^2$, we obtain

$$\begin{aligned} F_b^{(\mathrm{QA})} \approx{}& \exp\left[-\frac{\pi^2 2^{-2b}(n-b-1)+\delta}{2}\right] \\ &\times \exp\left[-6\sigma_{n,b}^2 - \frac{n\langle\Delta\varphi_0^2\rangle}{4}\right], \end{aligned} \tag{16}$$

where we assumed $b \geqslant 1$, leaving the π-gate part intact. Imposing the random hierarchy condition results in the fidelity of the banded adder

$$\begin{aligned} F_{\mathrm{RH,b}}^{(\mathrm{QA})} ={}& \exp\left[-\frac{\pi^2 2^{-2b}(n-b-1)+\delta}{2}\right] \\ &\times \exp\left[-\frac{6nb - 6b(b+1)/2 + 4n}{4(N/\pi)^2}\right], \end{aligned} \tag{17}$$

where $\delta = c(n-b-1) + d$ for $n > b+1$ denotes a small offset with fit constants c and d, which, in analogy to (6), takes residual correlations into account. Figure 8(b) shows that for the case of $b = 4$, e.g., with $c = -0.03$ and $d = -0.004$, together with the aforementioned term $[3(n-2) - 1]/(N/\pi)^2$

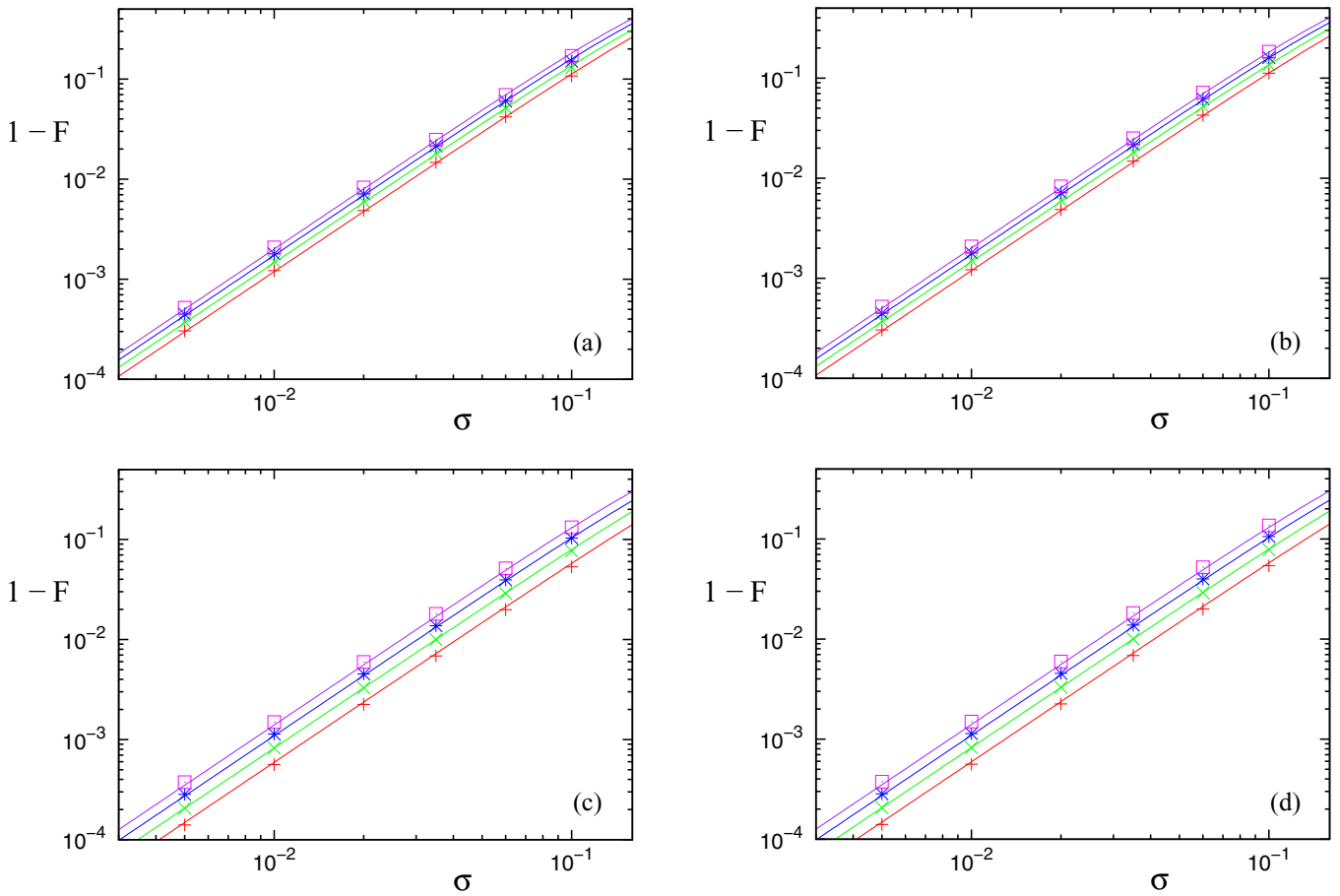

FIG. 9. (Color online) Complement $1-F$ of the fidelity F of the full-bandwidth quantum adder equipped with Gaussian-defective rotation gates $\tilde{\theta}_j$ as a function of the standard deviation σ of the gate errors. In order to match the random bit spectrum assumption used in the analytical calculations, all numerical simulation data are averaged over all possible integer input states $|\alpha\rangle$, where $\alpha = 0, \ldots, 2^n - 1$ and all possible integer addends $\nu = 0, \ldots, 2^n - 1$. Shown are the results of averaging over 10 000 realizations of the defects: (a) RC, (b) RU, (c) AC, and (d) AU. The cases with $n = 5$, 6, 7, and 8 correspond to pluses (red), crosses (green), asterisks (blue), and squares (purple), respectively.

added to the exponent, the analytical scaling relation $F_{\mathrm{RH,b}}^{(\mathrm{QA})}$ in Eq. (17) matches the numerical results in the practically interesting, small $1-F$ region to an excellent degree.

Following our detailed investigation of the effects and the scaling of the random hierarchy, we now apply our general scaling expressions to some additional, perhaps more conventional, models of gate errors. In Ref. [16], for instance, we investigated relative and absolute errors that may be correlated or uncorrelated with respect to the types j of the gates θ_j. For the relative correlated (RC), relative uncorrelated (RU), absolute correlated (AC), and absolute uncorrelated (AU) errors, respectively, following Eqs. (5)–(8) of [16], the defective rotation gates may be modeled as

$$\begin{aligned} &\text{(RC)} \quad \tilde{\theta}_j = \theta_j[1 + R_j(\sigma|\epsilon)], \\ &\text{(RU)} \quad \tilde{\theta}_j = \theta_j[1 + R(\sigma|\epsilon)], \\ &\text{(AC)} \quad \tilde{\theta}_j = \theta_j + R_j(\sigma|\epsilon), \\ &\text{(AU)} \quad \tilde{\theta}_j = \theta_j + R(\sigma|\epsilon), \end{aligned} \tag{18}$$

where $R_j(\sigma|\epsilon)$ or $R(\sigma|\epsilon)$ stand for Gaussian distributed random numbers with standard deviation σ or uniformly distributed random numbers between $-\epsilon$ and ϵ, respectively, where the presence or absence of the subscript j denotes the correlated or uncorrelated defects with respect to the rotation gate of type j.

To demonstrate the power of our general analytical scaling formulas (12) and (16) for the quantum adder fidelities, we are now going to derive the corresponding analytical fidelity scaling formulas for each of the eight error models specified in Eq. (18). In fact, these eight cases are covered by just four fidelity scaling formulas since, as proved in Ref. [16], there is no statistical difference between the correlated error models and the uncorrelated error models in Eq. (18).

We start with the case of Gaussian noise introduced into the full-bandwidth quantum adder and assume that the central limit theorem [28] holds for the phase-angle defects. Then, to first and zeroth order in n, the analytical fidelity scaling formulas for RC, RU, AC, and AU noise are given by

$$\begin{aligned} {}^{\mathrm{RC}}F_\sigma^{(\mathrm{QA})} &= {}^{\mathrm{RU}}F_\sigma^{(\mathrm{QA})} = {}^{\mathrm{R}}F_\sigma^{(\mathrm{QA})} \\ &\approx \exp\left\{-\left[\frac{6\pi^2(3n-4)}{144} + \frac{\lambda n\pi^2}{4}\right]\sigma^2\right\}, \end{aligned} \tag{19}$$

$$\begin{aligned} {}^{\mathrm{AC}}F_\sigma^{(\mathrm{QA})} &= {}^{\mathrm{AU}}F_\sigma^{(\mathrm{QA})} = {}^{\mathrm{A}}F_\sigma^{(\mathrm{QA})} \\ &\approx \exp\left\{-\left[\frac{6n(n-1)}{32} + \frac{\mu n}{4}\right]\sigma^2\right\}, \end{aligned} \tag{20}$$

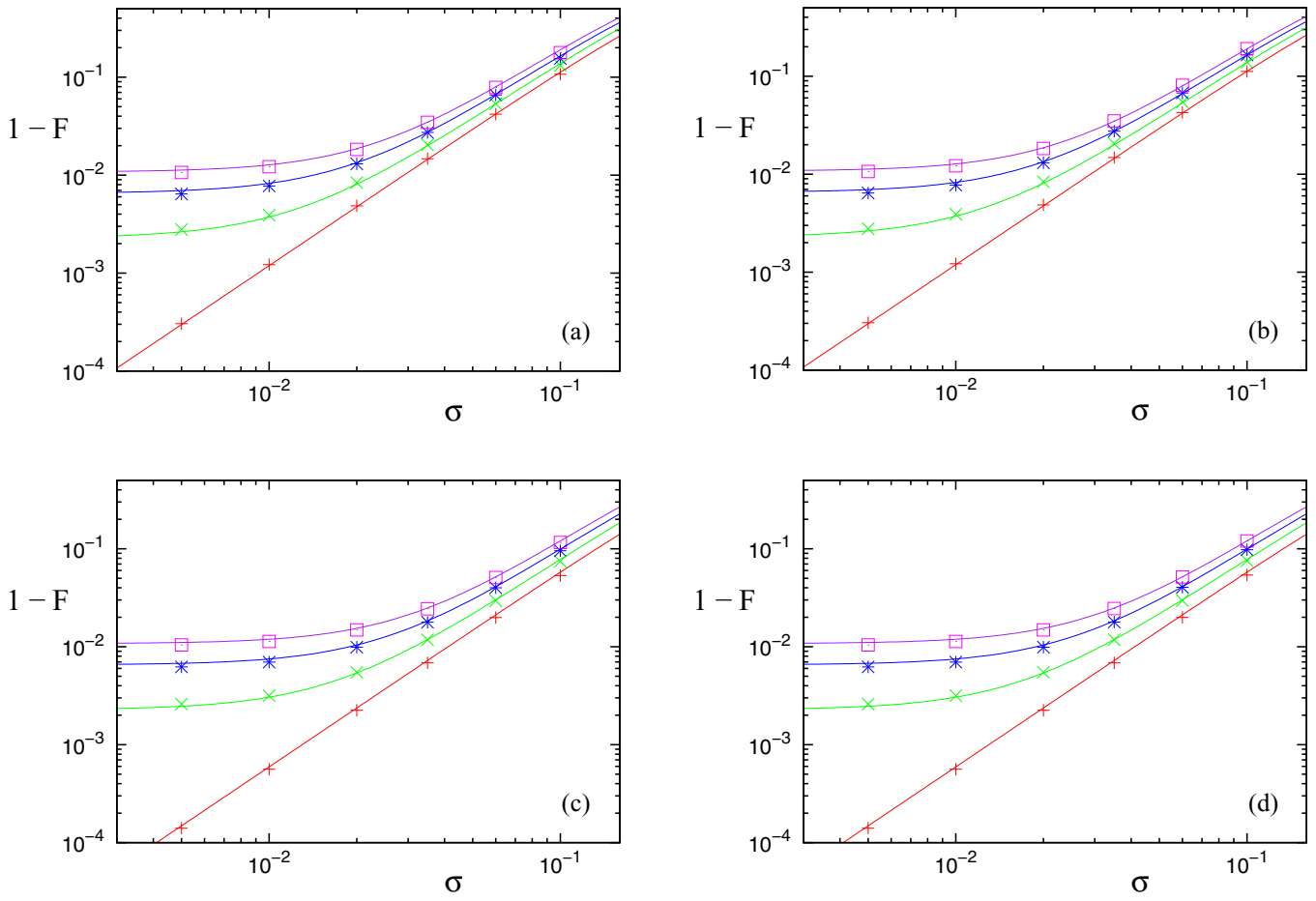

FIG. 10. (Color online) Complement $1-F$ of the fidelity F of the banded quantum adder (bandwidth $b=4$) equipped with the Gaussian-defective rotation gates $\tilde{\theta}_j$ as a function of the standard deviation σ of the gate errors. In order to match the random bit spectrum assumption used in the analytical calculations, all numerical simulation data are averaged over all possible integer input states $|\alpha\rangle$, where $\alpha=0,\ldots,2^n-1$ and all possible integer addends $\nu=0,\ldots,2^n-1$. Shown are the results of averaging over 10 000 realizations of the defects: (a) RC, (b) RU, (c) AC, and (d) AU. The cases with $n=5$, 6, 7, and 8 correspond to pluses (red), crosses (green), asterisks (blue), and squares (purple), respectively.

where the left superscripts RC,RU and AC,AU denote relative and absolute errors, respectively, and λ,μ are phenomenological constants. In Figs. 9(a)–9(d), for RC, RU, AC, and AU, respectively, plotting the complement $1-F$ of the fidelity vs the noise σ, we show the results of our numerical simulations (plot symbols) together with the analytical results (solid lines) according to (19) and (20) with $\lambda=3/5$ and $\mu=7/4$. We see that the numerical simulations and the analytical predictions agree to an excellent degree. In addition, our numerical simulations confirm that the correlated and uncorrelated cases are statistically equivalent.

We now turn to the case of Gaussian noise introduced into the banded quantum adder with bandwidth b. From (16) we obtain

$$ {}^{\mathrm{RC}}F_{\sigma,b}^{(\mathrm{QA})} = {}^{\mathrm{RU}}F_{\sigma,b}^{(\mathrm{QA})} = {}^{\mathrm{R}}F_{\sigma,b}^{(\mathrm{QA})} \approx \exp\left[-\frac{\pi^2 2^{-2b}(n-b-1)+\delta}{2}\right]\exp\left\{-\left[\frac{6\pi^2[(3n-4)-2^{-2b}(3n-3b-4)]}{144}+\frac{\lambda n\pi^2}{4}\right]\sigma^2\right\}, \tag{21}$$

$$ {}^{\mathrm{AC}}F_{\sigma,b}^{(\mathrm{QA})} = {}^{\mathrm{AU}}F_{\sigma,b}^{(\mathrm{QA})} = {}^{\mathrm{A}}F_{\sigma,b}^{(\mathrm{QA})} \approx \exp\left[-\frac{\pi^2 2^{-2b}(n-b-1)+\delta}{2}\right]\exp\left\{-\left[\frac{6[n(n-1)-(n-b)(n-b-1)]}{32}+\frac{\mu n}{4}\right]\sigma^2\right\}. \tag{22}$$

In Figs. 10(a)–10(d) we show the complement $1-F$ of the fidelity, comparing our numerical simulations (plot symbols) and our analytical results (solid lines) according to (21) and (22) for $b=4$, the same choices for λ and μ as in Fig. 9, and the same choice of δ as in Fig. 8(b). We see that our analytical fidelity scaling laws match the correspondent numerics to an excellent degree.

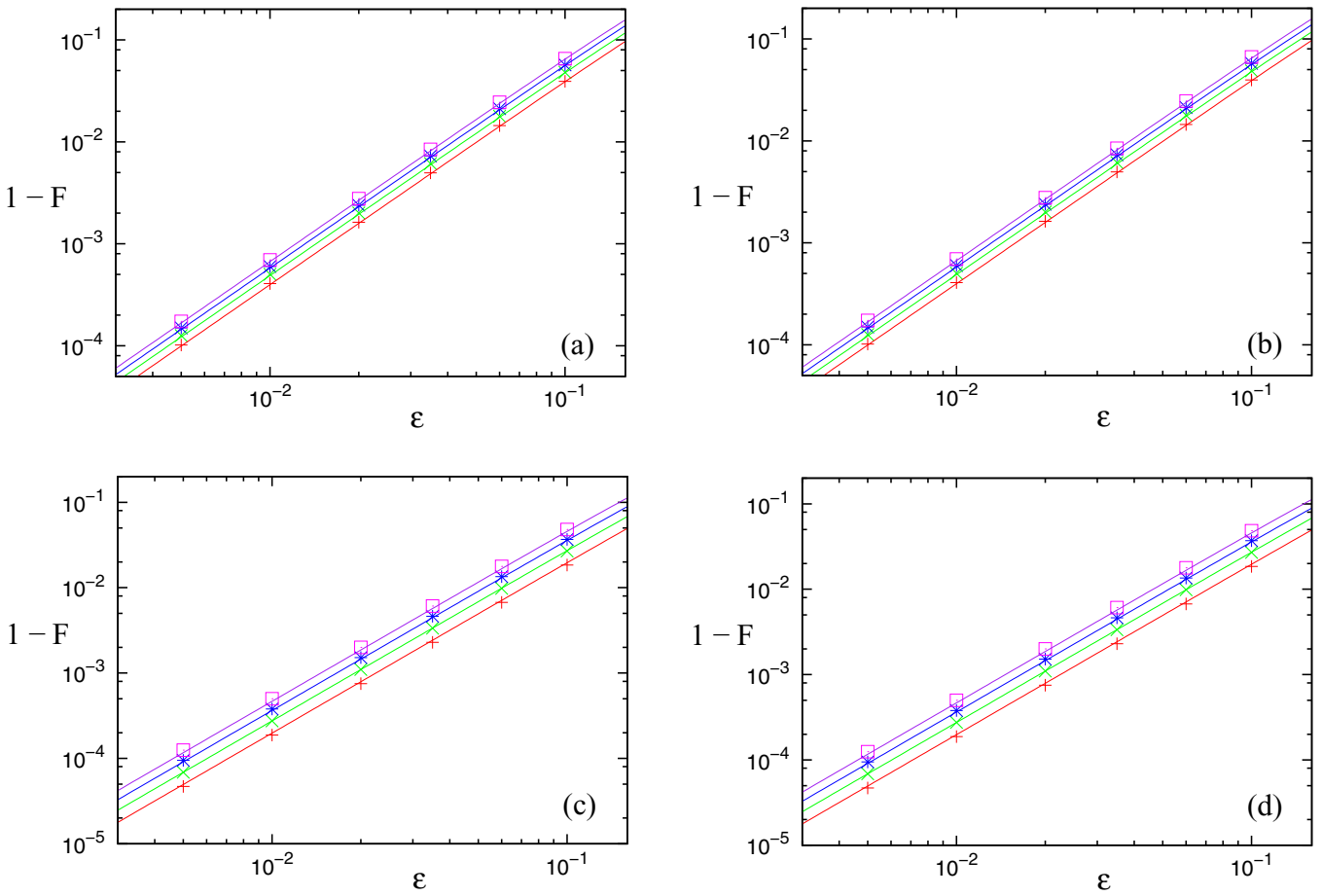

FIG. 11. (Color online) Complement $1-F$ of the fidelity F of the full-bandwidth quantum adder equipped with uniformly defective rotation gates $\tilde{\theta}_j$ as a function of the defect strength parameter ϵ. In order to match the random bit spectrum assumption used in the analytical calculations, all numerical simulation data are averaged over all possible integer input states $|\alpha\rangle$, where $\alpha = 0,\ldots,2^n-1$ and all possible integer addends $\nu = 0,\ldots,2^n-1$. Shown are the results of averaging over 10 000 realizations of the defects: (a) RC, (b) RU, (c) AC, and (d) AU. The cases with $n = 5$, 6, 7, and 8 correspond to pluses (red), crosses (green), asterisks (blue), and squares (purple), respectively.

Similarly, in Figs. 11(a)–11(d), corresponding to the cases RC, RU, AC, and AU, respectively, we plot the complement $1-F$ of the full-bandwidth adder fidelity

$$ {}^{\mathrm{RC}}F_{\epsilon}^{(\mathrm{QA})} = {}^{\mathrm{RU}}F_{\epsilon}^{(\mathrm{QA})} = {}^{\mathrm{R}}F_{\epsilon}^{(\mathrm{QA})} \approx \exp\left\{-\left[\frac{6\pi^2(3n-4)}{432}+\frac{\lambda n\pi^2}{12}\right]\epsilon^2\right\}, \tag{23} $$

$$ {}^{\mathrm{AC}}F_{\epsilon}^{(\mathrm{QA})} = {}^{\mathrm{AU}}F_{\epsilon}^{(\mathrm{QA})} = {}^{\mathrm{A}}F_{\epsilon}^{(\mathrm{QA})} \approx \exp\left\{-\left[\frac{6n(n-1)}{96}+\frac{\mu n}{12}\right]\epsilon^2\right\} \tag{24} $$

and in Figs. 12(a)–12(d) we plot the banded counterparts with bandwidth b,

$$ \begin{aligned} {}^{\mathrm{RC}}F_{\epsilon,b}^{(\mathrm{QA})} &= {}^{\mathrm{RU}}F_{\epsilon,b}^{(\mathrm{QA})} = {}^{\mathrm{R}}F_{\epsilon,b}^{(\mathrm{QA})} \\ &\approx \exp\left[-\frac{\pi^2 2^{-2b}(n-b-1)+\delta}{2}\right]\exp\left\{-\left[\frac{6\pi^2[(3n-4)-2^{-2b}(3n-3b-4)]}{432}+\frac{\lambda n\pi^2}{12}\right]\epsilon^2\right\}, \end{aligned} \tag{25} $$

$$ \begin{aligned} {}^{\mathrm{AC}}F_{\epsilon,b}^{(\mathrm{QA})} &= {}^{\mathrm{AU}}F_{\epsilon,b}^{(\mathrm{QA})} = {}^{\mathrm{A}}F_{\epsilon,b}^{(\mathrm{QA})} \\ &\approx \exp\left[-\frac{\pi^2 2^{-2b}(n-b-1)+\delta}{2}\right]\exp\left\{-\left[\frac{6[n(n-1)-(n-b)(n-b-1)]}{96}+\frac{\mu n}{12}\right]\epsilon^2\right\}, \end{aligned} \tag{26} $$

where this time the adder processor was subjected to uniform noise. As in the Gaussian noise cases, we chose $\lambda = 3/5, \mu = 7/4$ and the same form of δ as in Fig. 8(b). Our analytical results match the numerical results in Figs. 11 and 12 to an excellent degree.

For completeness we present here the formulas analogous to (19), (20), (23), and (24) for the full bandwidth QFT and (21), (22), (25), and (26) for the banded QFT, which we derived in complete analogy to our derivations of the corresponding quantum

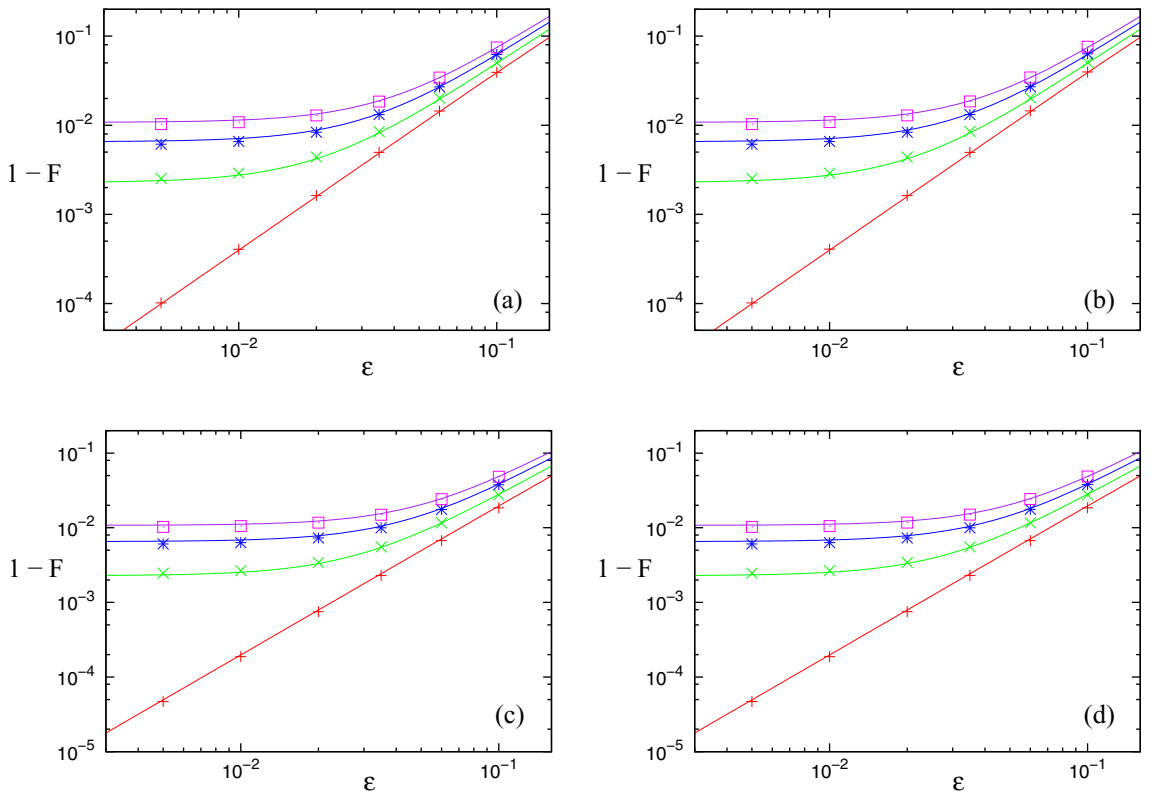

FIG. 12. (Color online) Complement $1-F$ of the fidelity F of the banded quantum adder (bandwidth $b=4$) equipped with the uniform-defective rotation gates $\tilde{\theta}_j$ as a function of the defect strength parameter ϵ. In order to match the random bit spectrum assumption used in the analytical calculations, all numerical simulation data are averaged over all possible integer input states $|\alpha\rangle$, where $\alpha=0,\ldots,2^n-1$ and all possible integer addends $\nu=0,\ldots,2^n-1$. Shown are the results of averaging over 10 000 realizations of the defects: (a) RC, (b) RU, (c) AC, and (d) AU. The cases with $n=5$, 6, 7, and 8 correspond to pluses (red), crosses (green), asterisks (blue), and squares (purple), respectively.

adder formulas. The QFT formulas (full bandwidth and banded) for relative and absolute Gaussian noise, respectively, are

$$ {}^{\mathrm{RC}}F_{\sigma}^{(\mathrm{QFT})} = {}^{\mathrm{RU}}F_{\sigma}^{(\mathrm{QFT})} = {}^{\mathrm{R}}F_{\sigma}^{(\mathrm{QFT})} \approx \exp\left[-\frac{\pi^2(3n-4)}{144}\sigma^2\right], \tag{27} $$

$$ {}^{\mathrm{RC}}F_{\sigma,b}^{(\mathrm{QFT})} = {}^{\mathrm{RU}}F_{\sigma,b}^{(\mathrm{QFT})} = {}^{\mathrm{R}}F_{\sigma,b}^{(\mathrm{QFT})} \approx \exp\left[-\frac{\pi^2 2^{-2b}(n-b-1)+\delta}{12}\right]\exp\left\{-\frac{\pi^2[(3n-4)-2^{-2b}(3n-3b-4)]}{144}\sigma^2\right\}, \tag{28} $$

$$ {}^{\mathrm{AC}}F_{\sigma}^{(\mathrm{QFT})} = {}^{\mathrm{AU}}F_{\sigma}^{(\mathrm{QFT})} = {}^{\mathrm{A}}F_{\sigma}^{(\mathrm{QFT})} \approx \exp\left[-\frac{n(n-1)}{32}\sigma^2\right], \tag{29} $$

$$ {}^{\mathrm{AC}}F_{\sigma,b}^{(\mathrm{QFT})} = {}^{\mathrm{AU}}F_{\sigma,b}^{(\mathrm{QFT})} = {}^{\mathrm{A}}F_{\sigma,b}^{(\mathrm{QFT})} \approx \exp\left[-\frac{\pi^2 2^{-2b}(n-b-1)+\delta}{12}\right]\exp\left[-\frac{n(n-1)-(n-b)(n-b-1)}{32}\sigma^2\right] \tag{30} $$

and the formulas for uniformly distributed noise, relative and absolute, respectively, are

$$ {}^{\mathrm{RC}}F_{\epsilon}^{(\mathrm{QFT})} = {}^{\mathrm{RU}}F_{\epsilon}^{(\mathrm{QFT})} = {}^{\mathrm{R}}F_{\epsilon}^{(\mathrm{QFT})} \approx \exp\left[-\frac{\pi^2(3n-4)}{432}\epsilon^2\right], \tag{31} $$

$$ {}^{\mathrm{RC}}F_{\epsilon,b}^{(\mathrm{QFT})} = {}^{\mathrm{RU}}F_{\epsilon,b}^{(\mathrm{QFT})} = {}^{\mathrm{R}}F_{\epsilon,b}^{(\mathrm{QFT})} \approx \exp\left[-\frac{\pi^2 2^{-2b}(n-b-1)+\delta}{12}\right]\exp\left\{-\frac{\pi^2[(3n-4)-2^{-2b}(3n-3b-4)]}{432}\epsilon^2\right\}, \tag{32} $$

$$ {}^{\mathrm{AC}}F_{\epsilon}^{(\mathrm{QFT})} = {}^{\mathrm{AU}}F_{\epsilon}^{(\mathrm{QFT})} = {}^{\mathrm{A}}F_{\epsilon}^{(\mathrm{QFT})} \approx \exp\left[-\frac{n(n-1)}{96}\epsilon^2\right], \tag{33} $$

$$ {}^{\mathrm{AC}}F_{\epsilon,b}^{(\mathrm{QFT})} = {}^{\mathrm{AU}}F_{\epsilon,b}^{(\mathrm{QFT})} = {}^{\mathrm{A}}F_{\epsilon,b}^{(\mathrm{QFT})} \approx \exp\left[-\frac{\pi^2 2^{-2b}(n-b-1)+\delta}{12}\right]\exp\left[-\frac{n(n-1)-(n-b)(n-b-1)}{96}\epsilon^2\right]. \tag{34} $$

IV. DISCUSSION

Our motivation for developing analytical scaling formulas is the fact that even the resources of the entire universe are insufficient for building a classical computer that would be capable of simulating a quantum processor in the regime of a large number of qubits [15]. Only analytical methods are powerful enough to explore this regime. Of course, if practical realizations of quantum processors were ideal, there is no need for additional simulations; the processor would perform according to the drawing-board specifications of its quantum circuit. However, by necessity, actual, practical realizations of quantum processors are constructed from hardware components that are not exact implementations of their circuit specifications, but will contain errors and defects. Therefore, a crucial question arises: How do these unavoidable defects influence the performance of quantum processors in a qubit regime that is inaccessible to classical simulation? For two examples of quantum processors, the QFT and the quantum adder, we answer this question by deriving analytical formulas for their performance when implemented with faulty rotation gates whose defects are described statistically with the help of several different error models that are close to what will be encountered in future large-scale quantum processors. Should it turn out that, in practice, the gate defects of these processors follow statistical laws different from those discussed in this paper, our analytical methods are powerful enough to encompass these cases as well. For given quantum hardware and its limitations it is essential for experimentalists and quantum engineers to be able to extrapolate the performance of a desired large-scale quantum processor before building it. This way it can be decided beforehand whether it makes sense to build the quantum processor with available quantum hardware, or whether such an endeavor is fruitful only after a new, more accurate generation of quantum hardware is available.

Quantum hardware defects are, of course, only one side of the issue. Decoherence [26] is the other performance-limiting factor. There are two reasons why we focus on quantum hardware defects first: (i) It is much more straightforward to provide analytically reliable and comprehensive performance estimates for defective quantum hardware than it is to accurately model and estimate decoherence effects and (ii) if it turns out that it is already unrealistic to realize a working quantum processor on the basis of available quantum hardware, it is not necessary to study decoherence effects. Therefore, it seems prudent to study the limiting effects of defective quantum hardware first and only then worry about decoherence. This course of action is in line with a similar recommendation by Landauer [29].

Naively one might think that since the action of any quantum processor is equivalent to the action of a large unitary matrix, and because of the linearity of matrix operations, small errors in the matrix elements should result in a small degradation of quantum-processor performance. That this linear thinking is not correct is clearly demonstrated by our fidelity formulas presented in Sec. III B, which show that quantum-processor performance decreases exponentially according to

$$F \sim \exp(-\alpha n^{\beta}\gamma^{2}), \tag{35}$$

where α and β are positive constants, n is the number of qubits, and $\gamma > 0$ is a measure of the size of the defects. This form of fidelity scaling is valid for both the QFT and the quantum adder.

In this connection we mention that it is not just a matter of waiting for the next generation of hardware. According to (35) the fidelity scales badly in the number of qubits n and thus implies a practical if not fundamental (e.g., natural transition line widths) limit on the number of qubits, even without considering decoherence. Since we need $F \gtrsim 0.1$ for acceptable quantum-processor performance, the exponent in Eq. (35) needs to be $\gtrsim -1$, which implies

$$\gamma \lesssim \frac{1}{\sqrt{\alpha n^{\beta}}}. \tag{36}$$

Obviously, for given practical or fundamentally achievable bounds on γ, this limit depends sensitively on the constants α and β, thus providing an additional reason for accurate scaling formulas in the large-n regime.

Our work is not the first to address hardware defects in quantum processors. Coppersmith [17] noticed that both the classical and quantum Fourier transforms incur only exponentially small errors if matrix elements (or quantum gates) with exponentially small rotation angles are deleted. Since this pruning operation of matrix elements (or quantum gates) results in a banded structure of the respective classical and quantum circuit diagrams, we called this pruning operation banding [15,19]. The banding idea, introduced by Coppersmith, was further developed, both analytically and numerically, by Fowler and Hollenberg [18], who showed that, assuming ideal quantum gates without defects, a bandwidth of $b = 8$ is sufficient for code-breaking applications. In Refs. [15,19], with simulations of QFT performance up to 40 qubits, we confirmed this result and provided additional analytical scaling relations.

While the possibility of banding is already a substantial boon for practical quantum-processor construction, since, instead of scaling quadratically in n for full bandwidth, the size of a given device with fixed bandwidth scales only linearly in the number of qubits n, the question remains of how gate defects in the remaining, active, gates affect quantum-processor performance. First numerical simulations addressing this point were performed by Cirac and Zoller [20], who considered the case of $n = 8$ qubits and assumed that all gates are active (no banding). The main result of this investigation was that an eight-qubit circuit is able to sustain an error level of up to 5%, i.e., this eight-qubit system was found to be robust with respect to gate errors. These calculations were extended by Miquel *et al.* [30] to a system with $n = 18$ qubits, again confirming robustness of the quantum processor. An analytical fidelity formula, similar in structure to (35) and based on a phase-diffusion model, was also provided.

Thus, the general idea of robustness of quantum processors with respect to gate defects, due to both banding and defects in the active quantum gates, is well established and has been around since about the mid 1990s. However, the general notion of robustness is not enough. As discussed in connection with (35), it has to be analyzed and carefully characterized in order to be able to exploit it experimentally and technologically. For instance, there is a qualitative difference between $\beta = 1$

and $\beta = 2$ in Eq. (35). In the first case, i.e., for $\beta = 1$, gate defects, even for quantum processors consisting of several thousand computational qubits, are relatively benign since the required gate accuracy, according to (36), scales like $1/\sqrt{n}$. In the second case, i.e., for $\beta = 2$, gate defects are more critical and, depending on α, may seriously limit the possible size of quantum processors.

While earlier published work focused on numerical investigations for a small number of qubits [20,30] or analytical and numerical investigations of banding that do not include gate defects [17,18], our work goes qualitatively beyond these works by providing asymptotic, reliable, analytical n-scaling formulas that can be used for processors consisting of thousands of qubits that simultaneously include banding and defects. In addition, with the help of numerical simulations, all of our formulas are carefully checked for accuracy in the classically accessible small-n regime.

While in our earlier work we investigated the effects of banding [15,19,27,31] and defects [16,22,23] *separately*, in this paper, we studied formulas including banding and defects *simultaneously*. Deriving these formulas required the development of a more powerful analytical technique. Furthermore, this technique is generally applicable to the computation of combined asymptotic scaling formulas for a wide range of defect models, which include simultaneous gate pruning (banding) and defects. These combined scaling formulas are not just the product of the fidelity for banding and the fidelity for the defects, separately. A nontrivial interference term exists that depends on both the bandwidth b and the defect strength (σ,ϵ), which dictates under which conditions, depending on the defect strength, banding is beneficial vs harmful. This term is qualitatively different and the crossover it predicts between the two regimes will be discussed in more detail at the end of this section. The existence of the interference between banding and defects was not anticipated and came as a surprise.

An additional surprise was provided by the results obtained from the random hierarchy error model. According to this model, rotation angles are generated randomly and the best matches for rotation angles required according to the circuit diagram are picked from a set S_N that contains N random rotation angles. Unlike in the more conventional error models, in which one perturbs around the exact rotation angles $\theta_j = \pi/2^j$, the randomly generated angles completely disregard the natural exponentially decreasing structure of θ_j with j and a rough hierarchy of angles, the random hierarchy, is achieved only via the process of selection of angles from the set S_N. This can result in tremendous errors for individual rotation gates, on the order of 50% and more, which, surprisingly, still yields perfectly acceptable quantum-processor performance. This takes the idea of robustness to a qualitatively different level and is distinct from our previous work, in which we only perturbed around the exact rotation angles. For us the viability of completely random gates, generated without any relation to the natural hierarchical structure of the exact gates, came as a complete surprise.

We investigated the random hierarchy model primarily for its academic value, providing a different gate defect model with extremely floppy gate angles, not guided by their natural structure. However, this model may also come in handy in certain experimental circumstances. As an example, consider the situation in which, for a certain hardware implementation of a certain quantum processor, it is natural and straightforward, for instance, because of the natural availability of atomic transition lines and laser frequencies, to produce without much effort a set S_N of rotation angles, which are not necessarily close to the target angles θ_j, but naturally uniformly distributed in angles. Then, according to the results of the random hierarchy model, even if the number N of angles in the set is small (on the order of 20), excellent performance of the quantum processor operated with these angles will result. This example shows how the set S_N may come about naturally and may lead to a valuable shortcut in the construction of the quantum hardware for realistic quantum processors.

So far in this paper we have investigated the fidelity of a QFT processor and a quantum adder processor in the presence of gate errors, both analytically and numerically. In particular, we focused on the random hierarchy, i.e., we draw approximate rotation gates that best match the exact rotation gates from a randomly generated set of numbers whose statistical distribution is uniform. The uniform distribution represents the larger gate angles relatively accurately, but completely misses the exponentially small angles (see Fig. 2). This might suggest that the uniform distribution is not appropriate and should be replaced with a distribution better tailored to the exponentially decreasing nature of the rotation angles in j. Following this line of reasoning, we replaced the uniform distribution in angle with a uniform distribution in j. We generate N random numbers that range from 0 to n and pick those that are closest to the integers ranging from 1 to $n-1$ to replace the integer parameter j of the exact gates, $\theta_j = \pi/2^j$, in an n-qubit QFT. Denoting the best approximate gates of θ_j as $\tilde{\theta}_j = \pi/2^{\xi_j}$, where the ξ_j are those random numbers drawn from the randomly generated set S_N of size N that best match j, we show in Fig. 13 the rotation gate angles θ_j (red

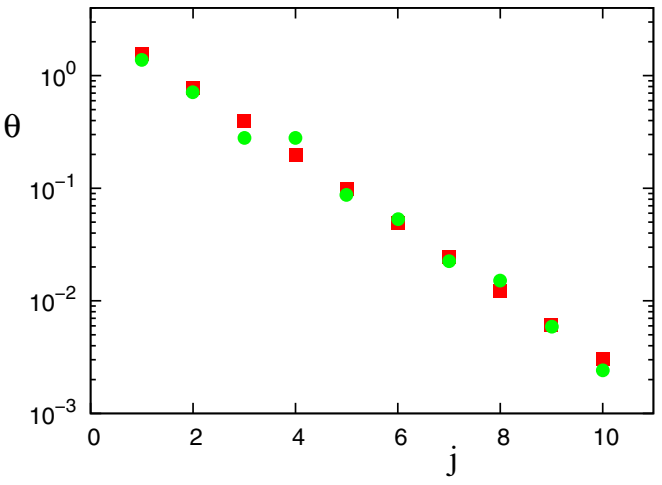

FIG. 13. (Color online) Exact rotation angles θ_j (red closed squares) compared with their corresponding approximations $\tilde{\theta}_j$ (green closed circles) as a function of qubit distance j for $j = 1,\ldots,10$. The approximations $\tilde{\theta}_j$ are the best matches for their corresponding θ_j, drawn from a set of $N = 20$ random numbers whose statistical distribution is uniform on an exponential scale ranging from 0 to n. Shown in the figure is the case of $n = 17$.

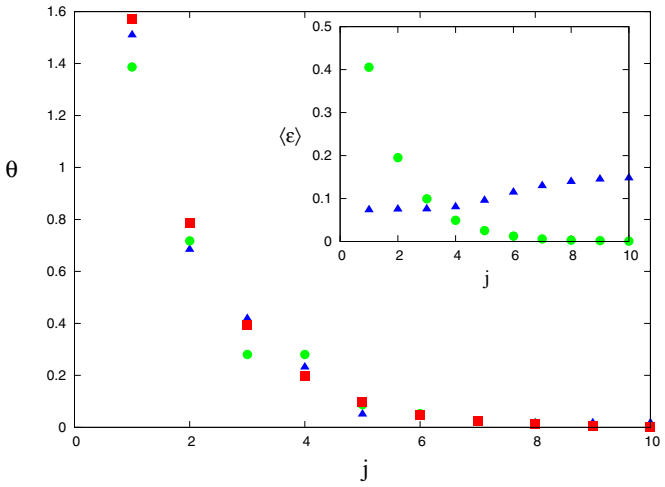

FIG. 14. (Color online) Exact rotation angles θ_j (red closed squares) compared with their approximations $\tilde{\theta}_j$ for the uniform (green closed circles) and exponential (blue closed triangles) hierarchies, as a function of qubit distance j for $j = 1, \ldots, 10$. Data are imported from Figs. 2 and 13 and plotted together on a linear scale for the convenience of the readers. The inset shows the averaged difference $\langle \epsilon_j \rangle = \langle |\tilde{\theta}_j - \theta_j| \rangle$ (green closed circles and blue closed triangles) for the uniform and exponential hierarchies, respectively, where averages were performed over 10 000 realizations of the random set S_N with $N = 20$ and $n = 17$ for each hierarchy.

squares) and $\tilde{\theta}_j$ (green circles) as a function of j, illustrating the result of the exponential random hierarchy for $N = 20$. As expected, we observe that, in comparison to the uniform random hierarchy (see Fig. 2), the exponential hierarchy better approximates the rotation gates with small rotation angles, i.e., large j, illustrated by the absence of a plateau for large j in Fig. 13 in contrast to Fig. 2.

On the other hand, guided by the robustness of the quantum processor with respect to banding [15,19], it is plausible to conjecture that in order to obtain higher fidelity, rotation gates θ_j with small j need to be more precisely approximated than gates with larger j values. This is justified because, as shown in our paper, the fidelity of the QFT processor subjected to rotation gate errors, for instance, is primarily determined by the *overall* phase angle error introduced to the processor, characterized by its variance. Considering that a mere 1% error of a $\theta_1 = \pi/2$ gate is equivalent to an 8% error of a $\theta_4 = \pi/16$ gate, given that there occur $n - j$ rotation gates θ_j acting on $n - j$ qubits of an n-qubit QFT processor, we note that, in order to achieve a large fidelity, much effort needs to be invested to make small-j rotation gates more precise. Figure 14 shows the same data shown in Figs. 2 and 13 for the uniform and the exponential hierarchy, respectively, but on a linear scale, magnifying the deviations between the exact gates and the random gates, which reveals the quality of each approximations as a function of j. For this particular realization of the hierarchies, the uniform hierarchy better approximates the gates with $j = 1$, 3, 4, and 6, while the exponential hierarchy better approximates the gates with $j = 2$, 5, and 7 onward.

However, in order to truly characterize the quality of approximations, one needs to perform averaging over ensembles of random numbers. Keeping the same conditions ($N = 20$ and $n = 17$) as the ones used in Fig. 14, we plot in the inset of Fig. 14 the difference $\epsilon_j = |\tilde{\theta}_j - \theta_j|$, where $\tilde{\theta}_j$ are the best approximates of θ_j produced according to the uniform or the exponential hierarchies, averaged over 10 000 ensembles of the random number set S_N, as a function of j. As expected, the uniform hierarchy better approximates the rotation gates θ_j with small j (large rotation angles) and the exponential hierarchy better approximates the rotation gates θ_j with large j (small rotation angles). In particular, on average the uniform ensemble represents the rotation angles of the first gate with an accuracy that is about 6 times better than the exponential ensemble, where the factor becomes 3 for the second gate and about 1.5 for the third gate. We also observe that there is a crossover between the two hierarchies at j between 3 and 4, i.e., for the current case of $N = 20$ and $n = 17$, the uniform hierarchy is better at approximating θ_j with $j \leqslant 3$ and the exponential hierarchy is better at approximating θ_j with $j \geqslant 4$. In addition, while the uniform hierarchy exhibits two plateaus at $\langle \epsilon \rangle \approx 0.07 \sim 0.08$ (see the inset of Fig. 14, small-j values) and 0.15 (see the inset of Fig. 14, large-j values), the exponential hierarchy case exhibits an exponential scaling of $\langle \epsilon \rangle \approx 0.8 \times 2^{-j}$ (fit not shown).

In order to explain the origins of these observations, we now turn to the following analytical analysis. Given N random numbers generated between 0 and n, the probability $P(d; N)$ to find a random number ξ_j between 1 and $n - 1$, inclusively, within a distance d of j, is $\sim[(n - 2d)/n]^N$, which, for $d \sim n/N$ and large N, may be written as $\exp(-2dN/n)$. This means that the approximate gate $\tilde{\theta}_j$ has the form $\pi/2^{j+r_j}$, where r_j is a random number distributed, up to normalization, according to the bivariate exponential function $\exp(-2dN/n)$.

Rewriting $\tilde{\theta}_j$ as $\pi/(2^j \times 2^{r_j})$, we see that, if r_j is sufficiently small or N is large enough, we may approximate $\tilde{\theta}_j \approx \theta_j[1 - \ln(2) r_j]$. Solving for $\epsilon_j = |\tilde{\theta}_j - \theta_j|$, then, since the ensemble average of r_j evaluates to $n/2N$, we obtain

$$\left\langle \epsilon_j^{\text{exp}} \right\rangle \approx \frac{\pi}{2N} \left[\frac{n \ln(2)}{2^j} \right], \tag{37}$$

where $\langle \cdots \rangle$ denotes an ensemble average.

Following the analysis shown in Sec. II B, i.e., $\epsilon_j = |\tilde{\theta}_j - \theta_j|$ follows a bivariate exponential distribution function that scales like $\sim \exp(-2Nd/\pi)$ for the uniform hierarchy, given θ_j is sufficiently larger than the error ϵ_j, we may write

$$\left\langle \epsilon_j^{\text{uni,bivariate}} \right\rangle \approx \frac{\pi}{2N}. \tag{38}$$

If, however, $\theta_j \lesssim \epsilon_j$, we may no longer use a bivariate distribution; rather, we must employ a univariate distribution in the limit $\theta_j \ll \epsilon_j$ since the best approximate angle $\tilde{\theta}_j$ will be larger than the exact angle θ_j. In this case, we obtain

$$\left\langle \epsilon_j^{\text{uni,univariate}} \right\rangle \approx \frac{\pi}{N}. \tag{39}$$

Evaluations of (37)–(39) with $N = 20$ and $n = 17$ match the previously discovered exponential and plateau behaviors of $\langle \epsilon_j \rangle$ in Fig. 14 to an excellent degree. In addition, the transition j that marks the crossover from the left to the right plateau in the uniform hierarchy case is correctly predicted by letting θ_j be comparable to $\epsilon_j \sim \pi/N$. Furthermore, equating (37) and

(38) yields the crossover

$$j_{\text{crossover}} = \frac{\ln[n\ln(2)]}{\ln(2)}, \tag{40}$$

below which the uniform hierarchy performs better than the exponential hierarchy in approximating θ_j and vice versa, which correctly predicts the aforementioned crossover shown in the inset of Fig. 14. We point out that (40) is independent of N, meaning, regardless of the size of the random set S_N, there always exists a critical n_c such that for $n > n_c$ a θ_j for a given j is always better approximated by the uniform hierarchy than the exponential hierarchy. In particular, the smaller the j, the smaller n_c is, implying a more favorable n-scaling relation of fidelity for the uniform hierarchy than for the exponential hierarchy.

To confirm that this is indeed true, once again, we start with $\tilde{\theta}_j \approx \theta_j[1 - \ln(2)r_j]$ for the exponential hierarchy. We see that this is identical to the RC noise investigated in Sec. III B for the quantum adder (see [16] for the case of the QFT), which can be shown to result in the QFT fidelity

$$F \approx \exp\left[-\frac{\pi^2\ln^2(2)}{36(2N)^2}n^2(3n - 4 + 2^{2-2n})\right]. \tag{41}$$

Consistent with our earlier expectations, this result shows that the QFT equipped with the exponential random hierarchy yields a fidelity scaling law, which, to leading order in n, is of the form $\ln(F) \sim -n^3$, one power in n worse than the results reported in Eq. (3), i.e., $\ln(F) \sim -n^2$, for the regular, uniformly distributed random hierarchy. Therefore, surprisingly, the exponential distribution performs worse than the uniform distribution. On the upside, this is good news for quantum engineering, since it is far more straightforward to realize uniformly distributed rotation angles than it is to realize exponentially distributed rotation angles. In addition, this result confirms our general rule that it is better to represent large rotation angles than small rotation angles, which here is expressed via the fact that the uniform distribution performs better than the exponential distribution. It also provides yet another example of the power of our analytical methods, which are able to deal successfully [see (41)] with a rather unconventional distribution of rotation angles (uniformly distributed in the exponents).

The least-favorable state $|2^n - 1\rangle$ plays a special role in our analytical derivations. It is the state that, statistically speaking, produces the worst results in terms of quantum-processor performance and therefore serves as a test state to produce a lower limit of processor fidelity. The following may be perceived as a problem with this procedure. When focusing on a particular realization of defective gates, i.e., a single copy of a quantum processor, it is possible that a particular state, different from $|2^n - 1\rangle$ but more adapted to a certain particular realization of gate defects, might actually yield results worse than $|2^n - 1\rangle$, while $|2^n - 1\rangle$ may actually be the most-favorable state. However, this scenario is statistically extremely unlikely. Therefore, without preknowledge of specific realizations of gate defects in an actually existing quantum processor, we have to assume that gate defects follow a statistical distribution, which requires us to average over many realizations of gate defects (typically hundreds or thousands, as done in this paper) to arrive at statistically meaningful conclusions. As shown in Fig. 3 and analytically proved in Appendix A, when ensemble averages are properly taken, $|2^n - 1\rangle$ is indeed the least-favorable state. The same considerations apply to the addend state $|2^n - 1\rangle$, which, in Appendix B, in conjunction with the state $|2^n - 1\rangle$, is shown to be the least-favorable addend state in the statistical sense.

The central theme of our paper is banding in the presence of defects. Intuitively, it is clear that it may be better to discard an obviously wrong gate rather than keep it. However, what is the formal criterion? What is the noise threshold that decides which gates to keep and which ones to discard? Based on the interference term, derived in this paper, between bandwidth and the size of the defects, we are able to answer these questions quantitatively.

Let us start with the Gaussian RC and RU cases defined in Sec. III B and address the following question: For a chosen fixed bandwidth b, for what values of σ is ${}^{\text{R}}F^{(\text{QFT})}_{\sigma,b} > {}^{\text{R}}F^{(\text{QFT})}_{\sigma}$? With (27) and (28) we obtain

$$\sigma > \frac{12}{\sqrt{6}}\sqrt{\frac{n-b-1}{n-b-4/3}} \approx 5. \tag{42}$$

This shows that in the case of relative errors the crossover between harmful banding and beneficial banding occurs only if σ is very large. Clearly, such large σ are uninteresting since, inserted in Eqs. (27) or (28), we obtain exponentially small fidelities. We conclude that in the case of relative errors, banding is never useful. This, however, requires that the relative errors in θ_j can be controlled at any level, which is experimentally impossible. Due to the exponentially decreasing nature of the rotation angles, experimentally, it becomes very quickly and completely impossible to distinguish θ_j from θ_{j+1} (say, $j > 20$) and thus to keep the relative errors at their prespecified levels. Therefore, for a sufficiently large number of qubits (e.g., $n > 20$), banding is always beneficial, experimentally. As a result, because of the limitation of experimental equipment, the model of absolute errors is more realistic.

In the case of absolute errors there is indeed a meaningful crossover between harmful and beneficial banding. We see this in the following way. Starting from (30), the maximum in performance corresponds to the minimum of the argument of the exponential functions in Eq. (30), viewed as a function of b for constant σ. Under the assumptions $n \gg 1$ and $n \gg b$, the minimum occurs at

$$b^{(\text{QFT})}_{\text{optimal},\sigma} = \frac{1}{2\ln(2)}\ln\left[\frac{8\pi^2\ln(2)}{3\sigma^2}\right]. \tag{43}$$

This criterion is independent of n and depends only logarithmically on σ. Therefore, even for the smallest reasonable σ, the criterion $b^{(\text{QFT})}_{\text{optimal},\sigma} < n - 1$ is easily fulfilled. For $\sigma = 10^{-3}$, e.g., we obtain $b^{(\text{QFT})}_{\text{optimal},\sigma} = 12$, compatible with banding estimates ranging from $b = 8$ [18] to $b = 22$ [32] for the QFT with perfect gates. The analogous formula for the quantum adder, obtained from (22), is

$$b^{(\text{QA})}_{\text{optimal},\sigma} = \frac{1}{2\ln(2)}\ln\left[\frac{8\pi^2\ln(2)}{3\sigma^2}\right], \tag{44}$$

identical to (43). Derived from (34) and (26), the formula analogous to (43) and (44) for optimal banding in the uniformly

distributed case is

$$b^{(\mathrm{QFT})}_{\mathrm{optimal},\epsilon} = b^{(\mathrm{QA})}_{\mathrm{optimal},\epsilon} = \frac{1}{2\ln(2)} \ln\left[\frac{8\pi^2 \ln(2)}{\epsilon^2}\right]. \quad (45)$$

In the case of the uniform and exponential hierarchies, the parameter N, i.e., the size of the random set S_N, takes the place of the error levels σ and ϵ and we may expect that, depending on N, there may also be a crossover between regions in which banding is helpful versus harmful. In general, we expect that banding is harmful if N is very large since in this case the rotation angles θ_j can be approximated with excellent accuracy. This is particularly clear in the limit of $N \to \infty$ since in this case all rotation angles are represented perfectly and any banding obviously reduces the performance of the corresponding quantum processor. However, for small N, banding may be helpful since in this case, in particular in the case of the uniform hierarchy, small rotation angles (large j) are not well approximated. Therefore, we expect the existence of a critical N_c below which (in N) banding is helpful and above which (in N) banding is harmful.

We use the full-bandwidth QFT fidelity scaling law (3) together with the banded QFT fidelity scaling law (6) to determine where the crossover between the helpful banding regime ($N < N_c$) and the harmful banding regime ($N > N_c$) occurs for the QFT. For given b, equating (3) and (6), and assuming small δ, we obtain

$$N_c^{(\mathrm{QFT,URH})} \approx 2^b \sqrt{\frac{3}{8}(n-b)}, \quad (46)$$

where URH stands for uniform random hierarchy. Now that we know how to compute N_c for given b, we would like to choose b as optimally as possible. Computing the maximum of the fidelity (6) as a function of b for fixed N, we obtain

$$b^{(\mathrm{QFT,URH})}_{\mathrm{optimal}} = \frac{1}{2\ln(2)} \ln\left[\frac{8\ln(2)N^2}{3}\right]. \quad (47)$$

As an example, for $N = 20$, used in Sec. II A, we obtain $b^{(\mathrm{QFT,URH})}_{\mathrm{optimal}} = 5$. Therefore, the bandwidths chosen in Figs. 4(b) and 5(b) are close to optimal.

A similar analysis can be done for the quantum adder as well. Equating (13) and (17) and assuming small δ and large n, we obtain

$$N_c^{(\mathrm{QA,URH})} \approx 2^b \sqrt{\frac{3}{2}(n-b)} \quad (48)$$

and, similar to the QFT case (47), the optimal bandwidth reads

$$b^{(\mathrm{QA,URH})}_{\mathrm{optimal}} = \frac{1}{2\ln(2)} \ln\left[\frac{2\ln(2)N^2}{3}\right]. \quad (49)$$

Although less useful in practice, for completeness, we provide here the corresponding formulas for the exponential random hierarchy. For the QFT we obtain

$$N_c^{(\mathrm{QFT,ERH})} \approx \frac{n\ln(2)}{2} \sqrt{1 - \frac{1}{3(n-b-1)}}, \quad (50)$$

$$b^{(\mathrm{QFT,ERH})}_{\mathrm{optimal}} = n - 1 + \frac{1}{2\ln(2)} - \frac{1}{3 - 12N^2/n^2\ln^2(2)} \quad (51)$$

and for the quantum adder, extending the domain from which we draw random numbers from $(0,n)$ to $(-1,n)$, we obtain

$$N_c^{(\mathrm{QA,ERH})} \approx \frac{(n+1)\ln(2)}{2} \sqrt{1 - \frac{1}{3(n-b-1)}}, \quad (52)$$

$$b^{(\mathrm{QA,ERH})}_{\mathrm{optimal}} = n - 1 + \frac{1}{2\ln(2)} - \frac{1}{3 - 12N^2/(n+1)^2\ln^2(2)}. \quad (53)$$

V. CONCLUSION

In this paper we investigated the fidelity of quantum processors subjected to rotation gate defects. In particular, we derived analytically the scaling of the fidelity of the QFT and the quantum adder processors equipped with randomly hierarchical gates. In addition, we derived analytical fidelity scaling laws for the quantum adder, subjected to gate errors with Gaussian or uniform distributions. Our analytical analysis, which matches numerical results to an excellent degree, shows that the QFT and the quantum adder processors are surprisingly robust against any type of gate errors in general and in particular against gate errors introduced according to the uniformly distributed random hierarchy, a particularly unfavorable type of defect, since it completely disregards the natural exponential ordering (hierarchy) of the rotation gates.

By demonstrating the extraordinary robustness of quantum processors with respect to hardware flaws, to the effect that the QFT and the quantum adder, e.g., still work even if most of their controlled-rotation gates are pruned and the surviving ones are implemented via selection from a randomly generated set, our work adds to the expectation that a quantum computer is a realizable and practical instrument that will change the paradigm of computation.

APPENDIX A: LEAST-FAVORABLE INPUT STATE FOR THE QFT

In this Appendix we show that the input state $|\psi_{\mathrm{in}}\rangle = |2^n - 1\rangle$ is the most-unfavorable integer input state for an n-qubit QFT, whose performance is measured in terms of the fidelity $F = |\langle\psi_{\mathrm{ideal}}|\psi_{\mathrm{actual}}\rangle|^2$. We start by invoking the approximate fidelity expression (2), which we can rewrite as

$$F \approx |\langle \exp[i\Delta\varphi(\alpha,\beta)]\rangle_\beta|^2, \quad (A1)$$

where $|\alpha\rangle$ is the integer input state of the QFT; β, an integer that ranges from 0 to $2^n - 1$, denotes the integer state spectrum of the output state of the QFT; $\langle\cdots\rangle_\beta$ stands for averaging over β; and $\Delta\varphi(\alpha,\beta)$ denotes the phase-angle defects associated with the n-qubit QFT with the input state $|\alpha\rangle$ and one of the output integer states $|\beta\rangle$. Since in this paper we focus attention on defective rotation gates with rotation angles $\tilde{\theta}_j = \theta_j + \Delta\varphi_j$, where the exact rotation angles are given by $\theta_j = \pi/2^j$, we may write

$$\Delta\varphi(\alpha,\beta) = \sum_{j=1}^{n-1} \sum_{l=1}^{n-j} \alpha_{[n-l]}\beta_{[j+l-1]}\Delta\varphi_j, \quad (A2)$$

where the subscripts $[n-l]$ and $[j+l-1]$ of α and β denote the $(n-l)$th and the $(j+l-1)$th binary digits of the integers

α and β, respectively. Inserting (A2) into (A1) and performing the β averaging by replacing $\beta_{[j+l-1]}$ by $1/2$, we obtain

$$F \approx \left| \exp\left(i \sum_{j=1}^{n-1} \sum_{l=1}^{n-j} \alpha_{[n-l]} \Delta\varphi_j / 2 \right) \right|^2 . \tag{A3}$$

At this point, we clearly see that, if all $\alpha_{[n-l]}$ are 1, we obtain the maximal variance of the phase-angle sum in Eq. (A3). In other words, we obtain the minimal fidelity. Hence, we conclude that $|\psi_{\text{in}}\rangle = |2^n - 1\rangle$ is indeed the input state of the n-qubit QFT, which incurs the maximal fidelity penalty.

APPENDIX B: LEAST-FAVORABLE INPUT STATE FOR THE QUANTUM ADDER

In the spirit of Appendix A, we show in this Appendix that the choice of $|\psi_{\text{in}}\rangle = |2^n - 1\rangle$ as input state and $|\nu\rangle = |2^n - 1\rangle$ as addend state is the most unfavorable combination of integer input and addend states for the n-qubit quantum adder whose performance is measured in terms of fidelity $F = |\langle\psi_{\text{ideal}}|\psi_{\text{actual}}\rangle|^2$. We start with the analytical fidelity expression (10) of the n-qubit quantum adder, which we can rewrite as

$$F^{(\text{QA})} \approx |\langle \exp[i\,\Delta\varphi(\alpha,\beta')] \rangle_{\beta'}|^2 |\langle \exp[i\,\Delta\varphi^{(\text{QFA})}(\beta';\nu)] \rangle_{\beta'}|^2 \times |\langle \exp\{-i\,\Delta\varphi[\beta', (\alpha+\nu) \bmod 2^n]\} \rangle_{\beta'}|^2, \tag{B1}$$

where, in analogy to the description of (A1), $|\alpha\rangle$ is the integer input state of the quantum adder; β', denoting the integer state spectrum of the intermediate state immediately following the QFT [the first operation of the quantum adder (see Fig. 6)], is an integer ranging from 0 to $2^n - 1$; $\langle \cdots \rangle_{\beta'}$ stands for averaging over β'; $\Delta\varphi(\alpha,\beta')$ denotes the phase angle defects associated with an n-qubit QFT with the input integer state $|\alpha\rangle$ and one of the integer output states $|\beta'\rangle$; and $\Delta\varphi^{(\text{QFA})}(\beta';\nu)$ denotes the phase-angle defects associated with an n-qubit quantum Fourier adder with addend $|\nu\rangle$ acting on the integer input state $|\beta'\rangle$. According to the gate operations of the quantum Fourier adder in Fig. 6, denoting by $\tilde{\theta}_j = \theta_j + \Delta\varphi_j$ the defective rotation angles, we may write

$$\Delta\varphi^{(\text{QFA})}(\beta';N) = \sum_{j=0}^{n-1} \sum_{l=1}^{n-j} \beta'_{[n-l]} \nu_{[n-l]} \Delta\varphi_j , \tag{B2}$$

which, together with $\Delta\varphi$ of the QFT in Eq. (A2), results in the adder fidelity

$$F^{(\text{QA})} \approx \left| \exp\left(i \sum_{j=1}^{n-1} \sum_{l=1}^{n-j} \alpha_{[n-l]} \Delta\varphi_j / 2 \right) \right|^2 \times \left| \exp\left(i \sum_{j=0}^{n-1} \sum_{l=1}^{n-j} \nu_{[n-l]} \Delta\varphi_j / 2 \right) \right|^2 \times \left| \exp\left(i \sum_{j=1}^{n-1} \sum_{l=1}^{n-j} [(\alpha+\nu) \bmod 2^n]_{[n-l]} \Delta\varphi_j / 2 \right) \right|^2 , \tag{B3}$$

where we performed the β' averaging and replaced all occurrences of binary bits of β' with $1/2$. At this point, we clearly see that, if the bit spectra of (i) α, (ii) ν, and (iii) $(\alpha + \nu)$ mod 2^n are as saturated as possible with 1, we obtain the minimal quantum adder fidelity. This is obtained when $\alpha = 2^n - 1$, $\nu = 2^n - 1$, and $(\alpha + \nu)$ mod $2^n = 2^n - 2$. This implies that the choice $|\psi_{\text{in}}\rangle = |2^n - 1\rangle$ and $|\nu\rangle = |2^n - 1\rangle$ is the combination of input and addend states for the quantum adder, which incurs the maximal fidelity penalty.

[1] P. W. Shor, in *Proceedings of the 35th Annual Symposium on the Foundations of Computer Science*, edited by S. Goldwasser (IEEE, Los Alamitos, 1994), pp. 124–134.

[2] R. Rivest, A. Shamir, and L. Adleman, Commun. ACM **21**, 120 (1978).

[3] F. Gaitan, *Quantum Error Correction and Fault Tolerant Quantum Computing* (CRC, Boca Raton, 2008).

[4] R. Barends, J. Kelly, A. Megrant, A. Veitia, D. Sank, E. Jeffrey, Y. Chen, B. Chiaro, J. Mutus, C. Neill *et al.*, Nature (London) **508**, 500 (2014).

[5] J. T. Muhonen, J. P. Dehollain, A. Laucht, F. E. Hudson, R. Karla, T. Sekiguchi, K. M. Itoh, D. N. Jamieson, J. C. McCallum, A. S. Dzurak, and A. Morello, Nat. Nanotech. (London) **9**, 986 (2014).

[6] A. G. Fowler, M. Mariantoni, J. M. Martinis, and A. N. Cleland, Phys. Rev. A **86**, 032324 (2012).

[7] M. Saffman and T. G. Walker, Phys. Rev. A **72**, 022347 (2005).

[8] R. Han, H. K. Ng, and B. G. Englert, arXiv:1407.8051v2.

[9] J. T. Muhonen, A. Laucht, S. Simmons, J. P. Dehollain, R. Kalra, F. E. Hudson, S. Feer, K. M. Itoh, D. N. Jamieson, J. C. McCallum, A. S. Dzurak, and A. Morello, J. Phys.: Condens. Matter **27**, 154205 (2015).

[10] J. Gulliksen, D. B. R. Dasari, and K. Molmer, EPJ Quantum Technol. **2**, 4 (2015).

[11] M. Veldhorst, J. C. C. Hwang, C. H. Yang, A. W. Leenstra, B. de Ronde, J. P. Dehollain, J. T. Muhonen, F. E. Hudson, K. M. Itoh, A. Morello, and A. S. Dzurak, Nat. Nanotechnol. **9**, 981 (2014).

[12] C. Zu, W.-B. Wang, L. He, W.-G. Zhang, C.-Y. Dai, F. Wang, and L.-M. Duan, Nature (London) **514**, 72 (2014).

[13] A. Abdumalikov, Jr., J. M. Fink, K. Juliusson, M. Pechal, S. Berger, A. Wallraff, and S. Filipp, Nature (London) **496**, 482 (2013).

[14] P. J. J. O'Malley *et al.*, Phys. Rev. Appl. **3**, 044009 (2015).

[15] Y. S. Nam and R. Blümel, Phys. Rev. A **87**, 032333 (2013).

[16] Y. S. Nam and R. Blümel, Phys. Rev. A **89**, 042337 (2014).

[17] D. Coppersmith, arXiv:quant-ph/0201067.

[18] A. G. Fowler and L. C. L. Hollenberg, Phys. Rev. A **70**, 032329 (2004).

[19] Y. S. Nam and R. Blümel, Phys. Rev. A **86**, 044303 (2012).

[20] J. I. Cirac and P. Zoller, Phys. Rev. Lett. **74**, 4091 (1995).

[21] I. García-Mata, K. M. Frahm, and D. L. Shepelyansky, Phys. Rev. A **78**, 062323 (2008).

[22] Y. S. Nam and R. Blümel, Quantum Inf. Comput. **15**, 721 (2015).

[23] Y. S. Nam and R. Blümel, Quantum Inf. Process. **14**, 1179 (2015).
[24] M. K. Thomsen, R. Glück, and H. B. Axelsen, J. Phys. A **43**, 382002 (2010).
[25] S. Beauregard, Quantum Inf. Comput. **3**, 175 (2003).
[26] M. A. Nielsen and I. L. Chuang, *Quantum Computation and Quantum Information* (Cambridge University Press, Cambridge, 2000).
[27] Y. S. Nam and R. Blümel, Phys. Rev. A **87**, 060304 (2013).
[28] A. Papoulis, *Probability, Random Variables and Stochastic Processes* (McGraw-Hill, New York, 1965).
[29] R. Landauer, in *Quantum Computing and Communications*, edited by M. Brooks (Springer, London, 1999), p. 61.
[30] C. Miquel, J. P. Paz, and W. H. Zurek, Phys. Rev. Lett. **78**, 3971 (1997).
[31] Y. S. Nam and R. Blümel, Phys. Rev. A **88**, 062310 (2013).
[32] N. D. Mermin, *Quantum Computer Science* (Cambridge University Press, Cambridge, 2007).